LASER BEAM COMBINING AND CLEANUP VIA STIMULATED BRILLOUIN SCATTERING IN MULTI-MODE OPTICAL FIBERS

THESIS

Blake C. Rodgers
First Lieutenant, USAF

AFIT/GAP/ENP/99M-09

DEPARTMENT OF THE AIR FORCE
AIR UNIVERSITY
AIR FORCE INSTITUTE OF TECHNOLOGY

Wright-Patterson Air Force Base, Ohio

AFIT/GAP/ENP/99M-09

LASER BEAM COMBINING AND CLEANUP VIA STIMULATED BRILLOUIN SCATTERING IN MULTI-MODE OPTICAL FIBERS

THESIS

Blake C. Rodgers
First Lieutenant, USAF

AFIT/GAP/ENP/99M-09

AFIT/GAP/ENP/99M-09

LASER BEAM COMBINING AND CLEANUP VIA STIMULATED BRILLOUIN SCATTERING IN MULTI-MODE OPTICAL FIBERS

THESIS

Presented to the Faculty of the School of Engineering

of the Air Force Institute of Technology

Air University

In Partial Fulfillment of the

Requirements for the Degree of

Master of Science in Applied Physics

Blake C. Rodgers, B.S.

First Lieutenant, USAF

March, 1999

AFIT/GAP/ENP/99M-09

LASER BEAM COMBINING AND CLEANUP VIA STIMULATED BRILLOUIN SCATTERING IN MULTI-MODE OPTICAL FIBERS

Blake C. Rodgers, B.S.

First Lieutenant, USAF

Approved:

Won B. Roh Chairman, Advisory Committee	Date
Craig Largent Member, Advisory Committee	Date
John R. Marciante Member, Advisory Committee	Date

Acknowledgements

I would like to thank several individuals whose help was invaluable to the completion of this thesis. I would like to thank my advisor, Dr. Won Roh, for his support and insight. I would also like to thank Captain Craig Largent and Dr. John Marciante for serving on my committee. Greg Smith was invaluable in his ability to find and fix the equipment needed for the research. Finally, I would like to thank my wife, Jennifer, for her never ending support and patience.

Table of Contents

List of Figures

Figure Page

Figure Page

List of Tables

Abstract

The main objective of this thesis was to demonstrate the feasibility of combining and cleaning up multiple laser beams via Stimulated Brillouin Scattering (SBS) in a multi-mode optical fiber. Beam combining via SBS in an optical fiber is of interest because of the low SBS threshold power in an optical fiber allowing low power diode laser beams to be combined into one high power beam. SBS theory and some of the important historical results are described briefly.

The experimental results clearly indicate that SBS in multi-mode optical fiber can indeed combine laser beams and clean up the beams at the same time. Both single-pass and ring-cavity geometries were used successfully. The SBS threshold power for the 9.5 μm diameter fiber was 26.5 ± 0.5 mW for a single-pass setup and 19.7 ± 0.5 mW for a ring cavity setup. The SBS power conversion slope efficiency was measured to be 42% for the single-pass setup and 52% for the ring-cavity. The SBS signal exhibited both periodic oscillations and random amplitude fluctuations, which are believed to be due to low levels of power used for the experiment. The polarization of the SBS signal was the same as the input laser beam.

The SBS and Stimulated Raman Scattering (SRS) gain coefficients for a 50 μm diameter fiber were also measured. The SBS gain coefficient measurement resulted in a value of 0.79 ± 0.44E-11 m/W. The SBS gain spectrum was also measured and the results yielded a full width at half maximum (FWHM) of 220 MHz. The measured SRS gain coefficient was 2.55 ± 0.05E-13 m/W at a wavenumber difference between the pump and the Stokes beams of 386.87 cm^{-1}.

Laser Beam Combining and Cleanup via Stimulated Brillouin Scattering in Multi-mode Optical Fibers

I. Introduction

The use of lasers has dramatically increased over the past few years. As the technology has matured, the Air Force has greatly increased its use of lasers. The Air Force 2025 forecast calls for a large role to be played by both ground and space based high power laser systems. The high power laser systems are of such great interest to the Air Force that two of the top ten future systems that are most wanted by the Air Force are high power laser weapon systems [1]. The Air Force is already beginning to see the use of high power lasers as weapons. Most notably, the Air Force has been developing the Air Borne Laser. While the development of the Air Borne Laser has been very successful so far, many problems exist. The biggest drawback to the Air Borne Laser is its size and weight. Chemical lasers, including that used for the Air Borne Laser, are very inefficient. Most chemical lasers have efficiencies less than 1 percent. Even the most efficient chemical laser system, the CO_2 laser, has an efficiency of approximately 27 percent [2:405]. These low efficiencies lead to the need for large amounts of energy to achieve even moderate power levels. This also increases the weight of a mobile high power laser system. Diode lasers, however, have efficiencies greater than 50 percent [2:442] and are very small and lightweight. While the high efficiency of diode lasers makes them a very appealing choice for air borne weapon systems, the maximum power of diode lasers is much lower than that of chemical lasers. For diode lasers to be an effective solution for

laser weapon systems, many diode laser beams must be efficiently combined. Some methods exist for combining laser beams, however, problems exist that limit their effectiveness. Many of these methods are not effective with diode lasers because of the low power output of individual diode lasers.

If an effective method for combining the laser beams of many diode lasers could be found, it would be an incredible asset to the Air Force. The diode lasers could be contained in a much smaller and lighter unit compared to a system like the Air Borne Laser and would use much less power. This would drastically decrease the size of air borne laser weapon systems making them more practical for both small aircraft and satellites. The major design problem that exists to make this type of system a reality is the efficient combining of the laser beams.

One likely solution to the problem of combining the beams is the use of Stimulated Brillouin Scattering (SBS) in optical fibers. SBS in optical fibers could potentially be used to combine hundreds of thousands of laser beams from diode lasers into one coherent high power beam. While the use of a fiber would limit the power of the combined beam, SBS in optical fibers would be ideal for a tactical situation in which the high power beam does not have to reach a target very far away.

Stimulated Brillouin Scattering is a nonlinear process that occurs in both optical fibers and bulk media. It involves the scattering of a laser beam from a variation in the refractive index, which is induced by the laser beam itself. The variation in the refractive index is created by electrostriction. In this process the regions of greater optical intensity compress, creating an acoustic wave that travels through the medium. The acoustic wave acts like a grating traveling at the velocity of the acoustic wave. The frequency of the

Stokes wave, the light that is reflected by the grating, is down shifted by the frequency of the acoustic wave. The three waves interact, leading to an exponential growth of the Stokes wave at the expense of the original laser beam [3:325-326].

Researchers have had some success in combining high power laser beams via SBS in bulk media. SBS in multi-mode optical fibers has been shown to act as a cleanup device for laser beams. The combination of these two results suggests that SBS in multi-mode optical fibers could be used to combine two or more laser beams to produce one coherent Gaussian beam.

While using SBS to cleanup and combine laser beams looks very promising, it is limited by the very narrow line width of the gain spectra which is characteristic of SBS. The narrow line width requires that the laser beams being combined are from single-mode lasers and are closer than 0.01 cm^{-1} in wavenumber. For a more practical system, the line width of the gain spectra should be much larger so multi-mode lasers can be used. The solution to the line width problem may be to use Stimulated Raman Scattering (SRS) instead of SBS. SRS is similar to SBS, but has a much larger line width. While the main focus of this thesis is the use of SBS for combining and cleaning up laser beams, the use of SRS in multi-mode fibers is considered briefly.

This research investigated the use of SBS in multi-mode optical fibers to combine and clean up laser beams. Some background information on optical fibers, SBS theory, and SRS theory will be presented in Chapter II. Chapter III presents some of the relevant results from previous research in this field. This is followed by the experimental setup in Chapter IV and the experimental results presented in Chapter V. Finally the conclusions are presented in Chapter VI.

II. Background

A general understanding of optical fibers, SBS theory, and SRS theory is needed before an understanding of this thesis material can be achieved. The basic properties of optical fibers will be presented below. This is followed by a presentation of the SBS theory and relevant equations. Finally a general overview of SRS is presented.

2.1 Optical Fibers

The basic properties of optical fibers will be presented in this section. These properties include fiber characteristics, coupling of light into optical fibers, fiber modes, effective length, and effective area.

There are two types of optical fibers. The simplest optical fiber is the step-index fiber. It consists of a core surrounded by a cladding material. The index of refraction of the cladding is slightly less than that of the core. This causes the light at certain angles to experience total internal reflection as shown in Figure 1. If the light enters at an angle

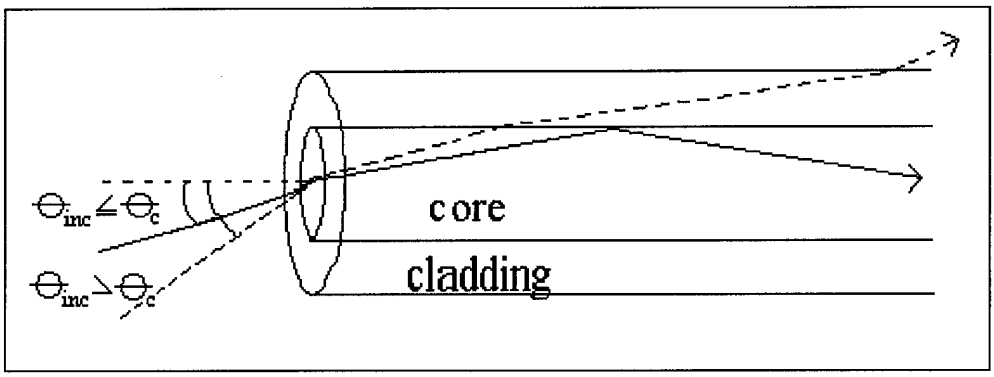

Figure 1. Light propagation in a step-index optical fiber.

less than or equal to the critical angle it will be guided down the fiber, otherwise the light will escape through the cladding. The second type of fiber is the graded-index fiber. In

the graded-index fiber, the index of refraction of the core decreases gradually away from the center of the core. The graded index fiber acts similar to the step-index fiber to guide the light down the fiber. The main difference in the graded index fiber is that the light is bent by the continuous change in the index of refraction instead of being reflected by the core-cladding boundary. This serves to redirect the light back to the center of the fiber. Since both types of fibers act in a similar way to guide the light and only step-index fibers were used for this thesis, the rest of the thesis will assume step-index fibers. In many cases, however, the equations presented are good for both types of fibers.

The incident angle limitation shown in Figure 1 can be determined from Snell's Law and the requirement that the light must experience total internal reflection to propagate down the fiber. The limitation on the angle, θ_{inc}, is given by

$$\theta_{inc} \leq \sin^{-1}(NA) \tag{1}$$

where NA is the numerical aperture. The numerical aperture is given by

$$NA = \sqrt{(n_{core})^2 - (n_{cladding})^2} \tag{2}$$

where n_{core} is the index of refraction of the fiber core, and $n_{cladding}$ is the index of refraction of the fiber cladding. Any light that enters the fiber at an angle greater than that defined in Equation 1 does not experience total internal reflection and will dissipate through the cladding.

To propagate the most light down the fiber, the light must be focused to a spot at least as small as the fiber core while still having an incident angle determined from

Equation 1. The lens used to couple the light into the fiber, therefore, has the focal length restriction

$$\frac{d_{beam}}{2NA} \leq f \leq \frac{d_{fiber}\, d_{beam}\, \pi}{4\lambda} \tag{3}$$

where d_{beam} is the diameter of the beam at the lens, d_{fiber} is the diameter of the fiber core, and λ is the wavelength of the laser.

The number of modes supported by the fiber is limited to

$$N \approx \frac{V^2}{2} \tag{4}$$

where the fiber parameter, V, is given by

$$V = \frac{d_{fiber}\, NA\, \pi}{\lambda} \tag{5}$$

Therefore, the number of modes the fiber supports is related to the square of both the fiber diameter and the wavelength of the light. Equation 4 is an approximation made with the assumption that the number of modes is large. For the fiber to support only 1 mode, the fiber parameter must be less than or equal to 2.405 [4:3].

The coupling efficiency is the percent of laser light that actually propagates down the fiber. This is determined by using a short piece of fiber ($\approx$ 2 meters). Measuring the light that exits this fiber is a good measure of the amount of light that was coupled into the fiber. The fiber is short enough that fiber losses have little effect, but still long enough that the light that was not launched at an angle small enough to be coupled into

the fiber escapes through the cladding before the end of the fiber. Dividing the power that exits the fiber by the power at the coupling lens gives the coupling efficiency. Doing this a number of times and taking the average gives a good estimate of the coupling efficiency for longer fibers with similar characteristics.

The actual length of the fiber must be adjusted to compensate for the losses in the fiber before using it to make calculations related to SBS. Thus, the effective length of the fiber is given by

$$L_{eff} = \frac{1 - \exp(-\alpha L)}{\alpha} \tag{6}$$

where α is the loss coefficient of the fiber given in the units of cm^{-1} and L is the actual fiber length [4:269]. The primary losses in the fiber are from absorption and Rayleigh scattering. This gives a loss coefficient that is primarily a function of wavelength. The loss for a particular fiber and a particular wavelength can be determined by measuring the intensity of the light transmitted by the fiber and the intensity of the light at the input coupling lens. The loss, α, is then given in cm^{-1} by

$$\alpha = \frac{-1}{L} \ln\left(\frac{I_{trans}}{C_0 I_{lens}}\right) \tag{7}$$

where C_0 is the coupling efficiency, I_{lens} is the intensity of the light at the coupling lens, and I_{trans} is the intensity of the light transmitted by the fiber. The value of the loss coefficient is usually given by the manufacturer.

The last important characteristic of optical fibers is the core area. By approximating the fundamental mode as a Gaussian, the effective area can be given as

$$A_{eff} = \pi w^2 \tag{8}$$

where w is the mode-width parameter determined from Figure 2 below.

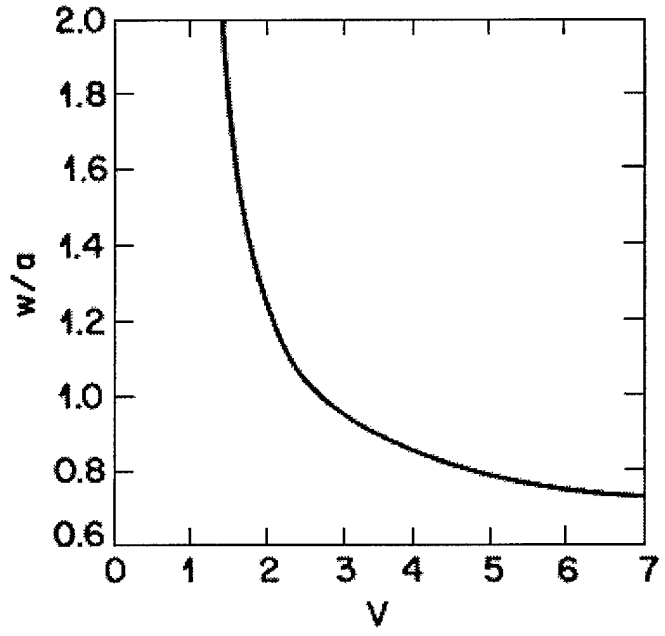

Figure 2. Variation of the mode-width parameter, w, with the fiber parameter, V [4].

2.2 Theory of Stimulated Brillouin Scattering

Stimulated Brillouin Scattering is a non-linear process that occurs in both optical fibers and bulk media. From a classical viewpoint it involves the scattering of a laser beam from a variation in the refractive index. The variation in the refractive index is created by electrostriction. In this process the regions of greater optical intensity compress, creating an acoustic wave that travels through the medium. The acoustic wave acts like a grating traveling at the velocity of the acoustic wave. The light that is reflected by the grating, the Stokes wave, is down shifted by the frequency of the acoustic

wave. The three waves interact, leading to an exponential growth of the Stokes wave at the expense of the original laser beam [3:325-328, 4:264].

From a quantum mechanical viewpoint, SBS can be viewed as the annihilation of pump photons and the subsequent creation of Stokes photons and acoustic phonons. From the conservation of energy and momentum, the frequency and momentum of each of the three waves are related by

$$\omega_A = \omega_P - \omega_S \tag{9}$$

$$\mathbf{k}_A = \mathbf{k}_P - \mathbf{k}_S \tag{10}$$

where ω_A, ω_P, and ω_S are the acoustic, pump and Stokes frequencies respectively, and $\mathbf{k}_A$, $\mathbf{k}_P$, and $\mathbf{k}_S$ are the acoustic, pump and Stokes wave vectors respectively. The acoustic frequency and wave vector must satisfy the dispersion relation given by

$$\omega_A = 2\, v_A\, |\mathbf{k}_P|\, \sin(\theta/2) \tag{11}$$

where v_A is the speed of sound and θ is the angle between the Stokes wave and the pump wave k vectors. For SBS in optical fibers, θ can only be 0 and 180 degrees because of the guiding nature of optical fibers. The Stokes light propagates in the direction opposite to the pump wave in isotropic media like optical fibers [4:264-265].

From Equation 9, the frequency shift between the Stokes wave and the pump wave is given by the frequency of the acoustic wave. Therefore, the frequency shift is given as

$$\nu_B = \frac{2nv_A}{\lambda_P} \tag{12}$$

where v_A is the speed of sound, n is the index of refraction and λ_P is the pump wavelength. For silica fibers, the speed of sound, v_A, is 5.96 km/s, and the index of refraction, n, is 1.45 [3:333, 4:265].

Once the Stokes wave is created, it grows exponentially at the expense of the pump wave. The growth of the Stokes wave at the expense of the pump wave can be described similar to stimulated emission by the equations

$$\frac{dI_S}{dz} = -g_B I_P I_S + \alpha I_S \tag{13}$$

$$\frac{dI_P}{dz} = -g_B I_P I_S - \alpha I_P \tag{14}$$

where I_S is the Stokes intensity, I_P is the pump intensity, α is the fiber loss, g_B is the Brillouin gain coefficient and z is the spatial coordinate [3:336, 4:268]. The gain experienced by the Stokes wave is characterized by the Brillouin gain coefficient. Assuming that the acoustic waves decay as $\exp(-t/T_B)$, where T_B is the phonon lifetime, the gain coefficient has a Lorentzian spectral profile which is given by

$$g_B(\nu) = \frac{(\Delta\nu_B/2)^2}{(\nu-\nu_B)^2 + (\Delta\nu_B/2)^2} g_B(\nu_B) \tag{15}$$

where $\Delta\nu_B$ is the full width at half maximum of the gain spectra. The maximum value of the Brillouin gain coefficient occurs at $\nu = \nu_B$ and is given by

$$g_B(\nu_B) = \frac{2\pi n^7 p_{12}^2}{c\lambda_P^2 \rho_0 \nu_A \Delta\nu_B} \tag{16}$$

where p_{12} is the longitudinal elasto-optic coefficient, and ρ_0 is the material density. Since $\Delta\nu_B$ is proportional to $1/\lambda^2$, the gain coefficient is not dependent on wavelength [3:336, 4:265]. For silica fibers, the gain coefficient at $\nu = \nu_B$ is 5E-11 m/W [4:269]. An example of the Brillouin gain spectra found by Tkach *et al.* in three different fibers is shown in Figure 3 below. The Brillouin line width in bulk silica is approximately 17

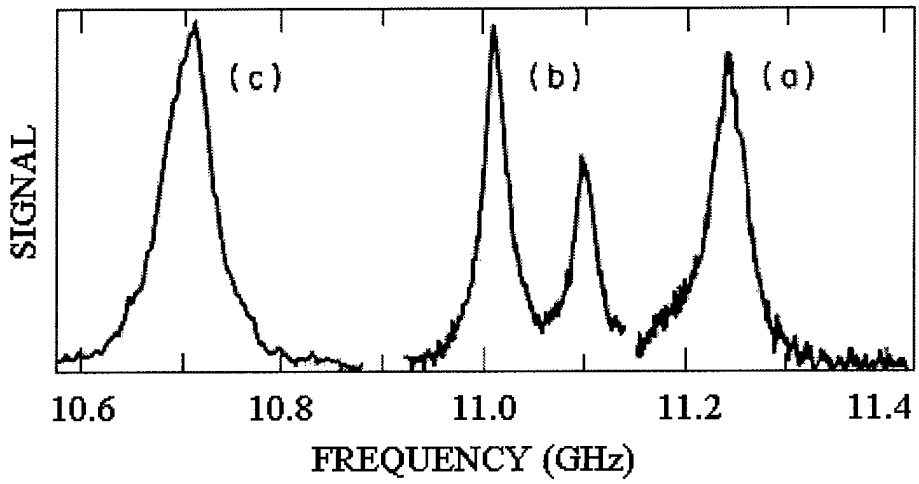

Figure 3. Brillouin gain spectra of three different fibers; λ_P=1.525 μm, (a) silica-core fiber, (b) depressed-cladding fiber, and (c) dispersion-shifted fiber [5].

MHz for a pump wavelength of 1.525 μm. In silica fibers, however, the Brillouin line width can be as high as 100 MHz for a pump wavelength of 1.525 μm. Since $\Delta\nu_B$ is proportional to $1/\lambda^2$, the expected $\Delta\nu_B$ for a pump wavelength of 807 nm would be 61 MHz with line widths as high as 350 MHz possible. The widening of the Brillouin gain profile is primarily a result of impurities and inhomogeneities in the fiber [5].

The maximum gain is reduced in the case of a pump with a spectral width exceeding the spectral width of the gain profile. For the specific case of a pump with a

Lorentzian spectral profile and a spectral width exceeding the width of the gain profile, the maximum Brillouin gain is given by

$$\tilde{g}_B = \frac{\Delta\nu_B}{\Delta\nu_B + \Delta\nu_P} g_B(\nu_B) \tag{17}$$

where $\Delta\nu_P$ is the full width at half maximum of the pump [6].

Once the gain coefficient is determined, the expected Stokes intensity and the SBS threshold power can be calculated. An approximation to the Stokes intensity can be made by solving Equation 13 and 14 neglecting pump depletion. The Stokes intensity is then given by

$$I_S(0) = I_S(L)\exp\left(\frac{g_B P_0 L_{eff}}{A_{eff}} - \alpha L\right) \tag{18}$$

where P_0 is the pump power at the input end of the fiber (z = 0), $I_s(L)$ is the input Stokes intensity at the far end of the fiber (z = L). Equation 18 shows how a fictitious photon injected at z = L grows exponentially, gaining its power from the pump. In most cases instead of injecting the fictitious photon into the fiber, SBS starts from noise and spontaneous Brillouin scattering. Once the SBS starts, it grows according to Equation 18. If the pump power is below the threshold power, the fiber loss will dominate, fictitious the photons will decay, and no SBS will occur. The threshold power required to achieve SBS is given by

$$\frac{g_B P_0^{th} L_{eff}}{A_{eff}} \cong 21 \tag{19}$$

where P_0^{th} is the threshold pump power coupled into the fiber at z = 0. In many cases the effective area, A_{eff}, can be approximated by the area of the fiber core [7]. The value of 21 can vary by a factor between 1 and 2 depending on how well the fiber maintains the polarization of the light. For complete depolarization, the value of 42 is used instead of 21 [4].

While Equation 18 is useful for estimating the Stokes intensity, it is inaccurate because it does not account for the depletion of the pump beam. To account for pump depletion, Equations 13 and 14 must be solved exactly. Assuming the pump power is above the SBS threshold, Tang gives the analytical solution including pump depletion as

$$I_S(z) = \frac{b_0(1-b_0)}{G(z)-b_0} I_P(0)\exp(-\alpha z) \tag{20}$$

$$I_P(z) = \frac{(1-b_0)G(z)}{G(z)-b_0} I_P(0)\exp(-\alpha z) \tag{21}$$

where

$$b_0 = \frac{I_S(0)}{I_P(0)} \tag{22}$$

$$g_0 = g_B I_P(0) \tag{23}$$

$$G(z) = \exp\{(1-b_0)\frac{g_0}{\alpha}[1-\exp(-\alpha z)]\} \tag{24}$$

In the above equations, b_0 is a measure of the Brillouin efficiency and g_0 is the small-signal gain coefficient [8]. If the pump power is not above the SBS threshold power, Equations 13 and 14 must be solved numerically.

Once the pump power is above the SBS threshold, the Stokes wave is created. The Stokes and pump waves interact along the effective length of the fiber to result in an

exponential growth of the Stokes wave at the expense of the pump wave. Since the growth of the Stokes wave is dependent on the pump power, the majority of the growth occurs in the first quarter of the fiber creating oscillations in the Stokes wave intensity. The oscillations have a period equal to twice the transit time of a photon traveling from one end of the fiber to the other. The large growth of the Stokes wave at the input end of the fiber depletes the intensity of the pump wave. As the depleted pump wave travels to the other end of the fiber, the growth of the Stokes wave is reduced. The resulting Stokes wave has a lower intensity as it exits the fiber. As the resulting Stokes wave travels out the input end of the fiber, the pump returns to a high intensity, increasing the growth of the Stokes wave in the fiber, and the process begins again. This gives the period of oscillation of twice the photon transit time down the length of the fiber. If the fiber is closed in on itself to create a ring, the SBS oscillations will have a period corresponding to the photon transit time around the ring. Once the pump power is far above the SBS threshold power, Equation 18 is valid and no oscillations should occur [4:272]. The stability condition of the SBS wave is expressed graphically in Figure 4.

2.3 Theory of Stimulated Raman Scattering

SRS is similar to SBS in its effects. SRS is a nonlinear process that involves the scattering of photons by molecules to lower frequency photons. At the same time, the molecule transitions to a higher vibrational state. Similar to SBS, the scattering process creates a Stokes wave that is down shifted in frequency from the pump wave. Also as with SBS, the Stokes wave grows exponentially at the expense of the pump wave. There are, however, a number of differences between SBS and SRS. Most notably is the large frequency difference between the pump and Stokes waves and the very broad gain

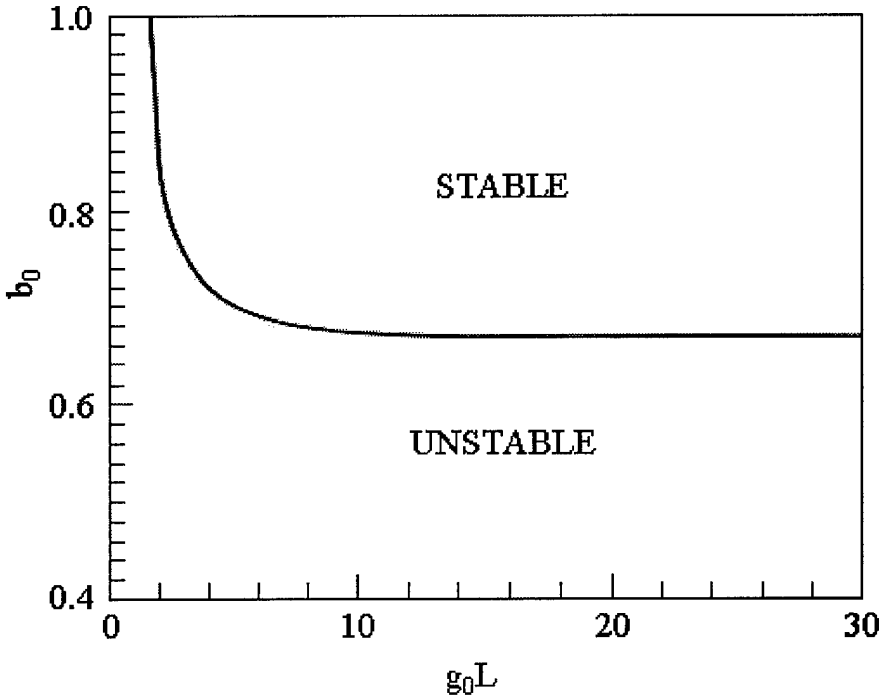

Figure 4. Stable and unstable regions of SBS. Below the critical value of the relative Stokes intensity [$b_0 = I_S(0)/I_P(0)$], the steady state is unstable as a function of the gain factor g_0L ($g_0 = g_B I_P(0)$) [9].

spectra compared to that of SBS. SRS is also characterized by a maximum gain coefficient that is typically two orders of magnitude smaller than the maximum gain coefficient of SBS. Finally, SRS can occur in both the forward and backward directions, while SBS only occurs in the backward direction.

The growth of the Stokes wave and the interaction of the Stokes and pump waves for backward SRS are described by

$$\frac{dI_S}{dz} = -g_R I_P I_S + \alpha_S I_S \tag{25}$$

$$\frac{dI_P}{dz} = -\frac{\omega_P}{\omega_S} g_R I_P I_S - \alpha_P I_P \tag{26}$$

were α_P is the loss coefficient for the pump wave, α_S is the loss coefficient for the Stokes wave, g_R is the Raman gain coefficient, ω_P is the frequency of the pump wave, ω_S is the frequency of the Stokes wave, I_P is the pump intensity, and I_S is the Stokes intensity. The two different loss coefficients are a result of the large wavenumber difference between the pump and Stokes wave. For pure silica at the maximum gain, the pump and Stokes waves differ by approximately 440 cm^{-1} [4:220-221].

The SRS threshold power is given by

$$\frac{g_R P_{th} L_{eff}}{A_{eff}} \cong 16 \tag{27}$$

where L_{eff} is given by Equation 6, g_R is the Raman gain coefficient and A_{eff} is the effective area. Similar to SBS, once the pump power is above the threshold power, the SRS Stokes wave grows exponentially at the expense of the pump wave [4:223].

As mentioned above, the SRS gain spectra is typically much broader than the SBS gain spectra. The Raman spectrum found by Stolen for fused silica at a pump wavelength of 1 μm is shown in Figure 5. A comparison of Figure 3 with Figure 5 shows the large difference in the gain spectra of SBS and SRS. The value of the maximum Raman gain coefficient scales inversely with the pump wavelength [4:220]. In silica fibers, this gives a maximum SRS gain coefficient of 1.2E-13 m/W for a pump wavelength of 807 nm.

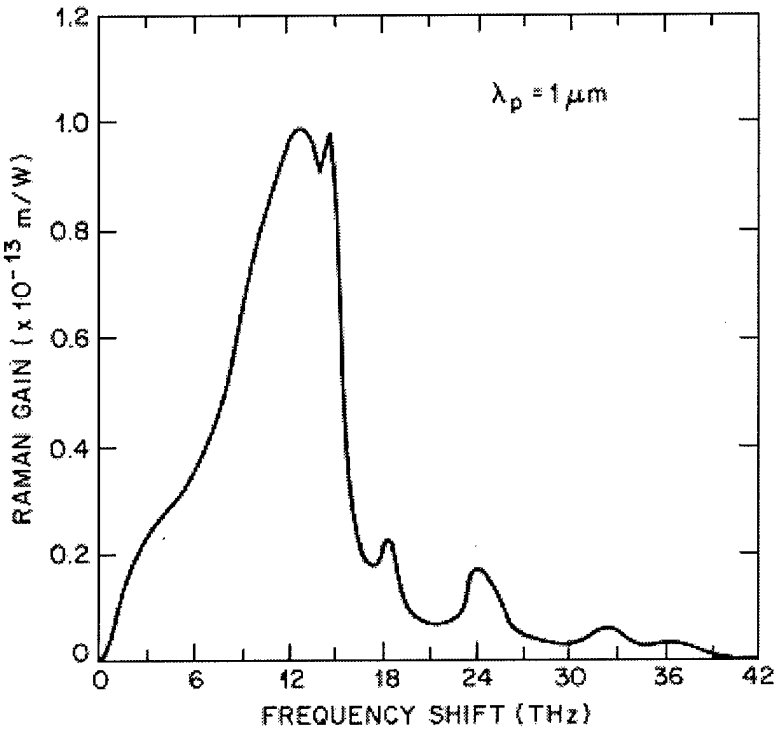

Figure 5. Raman gain spectrum for fused silica at a pump wavelength of 1 μm [10].

III. Historical Results

SBS has been extensively investigated since its first observation in 1964. This chapter will present some of the more notable research performed since it was first observed. Since so much research has been performed in this area of study, only a few of the many results can be presented here. Therefore, the research presented below is concentrated on the research that is most applicable to this thesis. A more in depth resource into the history and theory of SBS can be found in Chapter 9 of *Nonlinear Fiber Optics* by Agrawal.

SBS was first observed in 1964 in quartz and sapphire by Chiao *et al.* [11]. Ippen and Stolen first observed SBS in optical fibers in 1972. A pulsed Xenon laser (λ = 535.5 nm) was used as the pump laser. Using a 5.8 meter fiber with a core diameter of 3.8 μm, the threshold power was observed to be 2.3 W. Longer fibers were also investigated and found to have a threshold power below 1 W [7]. The lower power threshold that was found in longer fibers suggested a limitation on optical communications. This limitation on optical communications led Cotter [12], N. Uesugi *et al.* [13] and others to investigate SBS in single-mode fibers of length 4 to 32 kilometers. Cotter found the threshold to be as low as 5 mw and the SBS conversion efficiency to be 65% for the 32 km fiber [12]. A plot of Cotter's results showing the output power as a function of input power is shown in Figure 6.

Other properties of SBS in optical fibers were observed by Bar-Joseph *et al.* [9]. They showed that in the presence of external feedback, the SBS intensity oscillates. Gaeta *et al.* further investigated the fluctuations in the SBS intensity. They found that when the power is many times the threshold power, the fluctuations in the SBS intensity

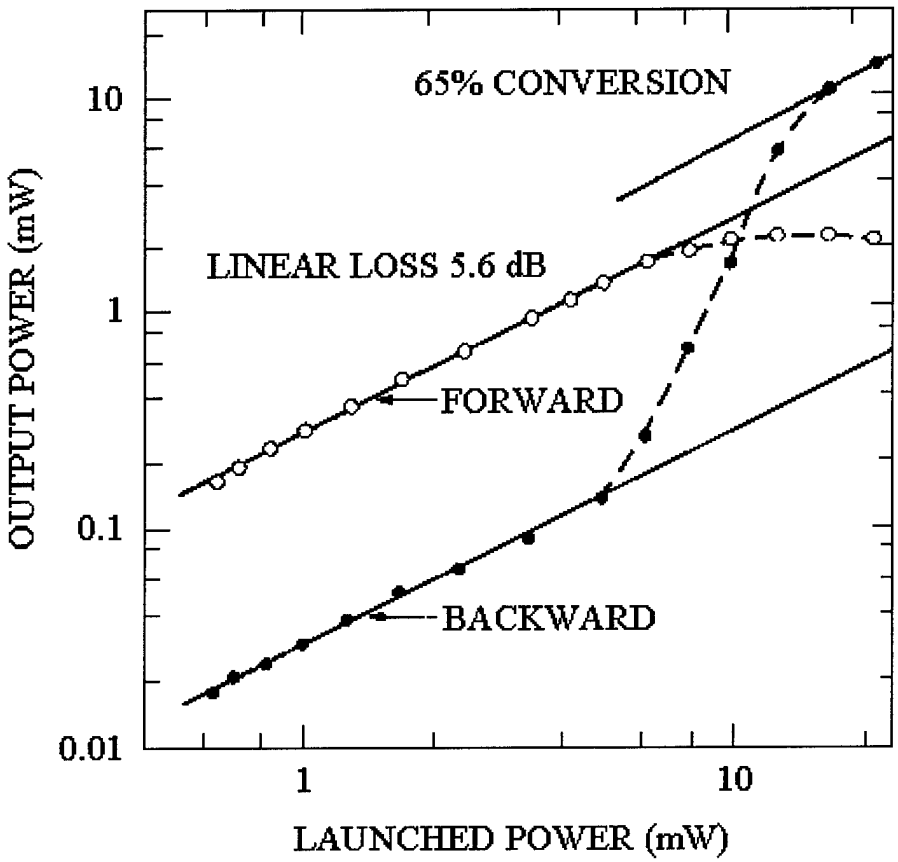

Figure 6. Power transmitted (forward) and backscattered (backward) from a 13.6 km single-mode fiber as a function of launched power [12].

are suppressed as discussed in Chapter II [14]. Harrison *et al.* found that SBS in the absence of external feedback exhibited fully developed chaos. In the presence of external feedback, the SBS dynamics exhibit both chaos and stable oscillations [15].

The low power threshold for SBS in optical fibers has prompted a large amount of research into ways to prevent SBS in optical communications systems. Others, however, have found applications to take advantage of the properties of SBS in optical fibers. One application for SBS that has been investigated is the use of SBS in optical fibers as a laser gain medium. Hill *et al.* reported the first observation of continuous wave SBS laser

action in an optical fiber ring cavity in 1976. The 9.5 meter single-mode fiber used had losses less than 100 dB/km and a core diameter of 2.4 μm. The fiber ring was pumped with an Argon laser (λ = 514.5 nm). The Brillouin laser had an output of 20 mW [16]. Since this was first demonstrated, Ponikvar *et al.* [17], Stokes *et al.* [18], and numerous others have investigated both continuous wave and pulsed operation of Brillouin fiber ring lasers.

Phase conjugation involves the reversal of the direction and spatial portion of the phase factor of a light wave [19:8]. It has become a useful method for cleaning up an aberrated laser beam. Laser beam combining using SBS phase conjugation in bulk material was first investigated by Basov *et al.* in 1980 [20]. Valley *et al.* [21], Loree *et al.* [22], and others have also successfully phase locked two or more laser beams using SBS phase conjugation. Sternklar *et al.* have shown that there is a 1 mrad tolerance in the beam alignment when using SBS in bulk media to combine and phase lock two laser beams [23]. SBS phase conjugation in optical fibers was first observed by Kuzin *et al.* in 1982 [24].

More recently, Bruesselbach investigated SBS in long fibers with a few to several hundred modes. The fibers were observed to act as beam cleanup devices through the use of SBS. The SBS output from the fiber was observed to come from only the primary mode, HE_{11}. Phase conjugation did not occur. The pump power was efficiently transferred to the SBS output creating a clean laser beam [25].

IV. Experimental Setup

This chapter presents the experimental setup and the procedures used. The chapter is separated into the equipment and procedures common to all experimental setups used, the single laser beam setup, the beam combination setup, and the gain measurement setup.

4.1 Equipment and Procedures

For the experiments performed, four Spectra Diode Labs diode lasers were used. Three of the lasers were 150 mW single-mode lasers, while the third was a 100 mW single-mode laser. The 100 mW laser had a wavelength of 808 nm. The wavelengths of the three 150 mW lasers were 807 nm, 809 nm, and 831 nm, respectively. The wavelengths could be varied over approximately one to two nanometers by varying the current and the temperature of the diode laser. The basic experimental setup is shown in Figure 7. All of the lasers were polarized in the horizontal direction. The lasers were collimated using a 20X near infra-red (NIR) coated objective lens. The lasers were isolated with Optics for Research IO-5 Wideband Optical Isolators with 35 to 41 dB of isolation. The optical isolator prevented most of the SBS signal from reaching the laser.

The laser and SBS frequencies were monitored with a Burleigh Fabry-Perot Interferometer in conjunction with a Burleigh WA-10 Wavemeter. The interferometer had a free spectral range of 8 GHz and a finesse of approximately 200. The wavemeter gave the wavenumber to within 0.01 cm^{-1}. The wavemeter had the limitation that the input signal could not have more than 30 percent amplitude noise.

The optical fiber used for all experiments except the gain measurement was a single-mode fiber for 1.3 μm to 1.5 μm made by Corning. The fiber was a silica core

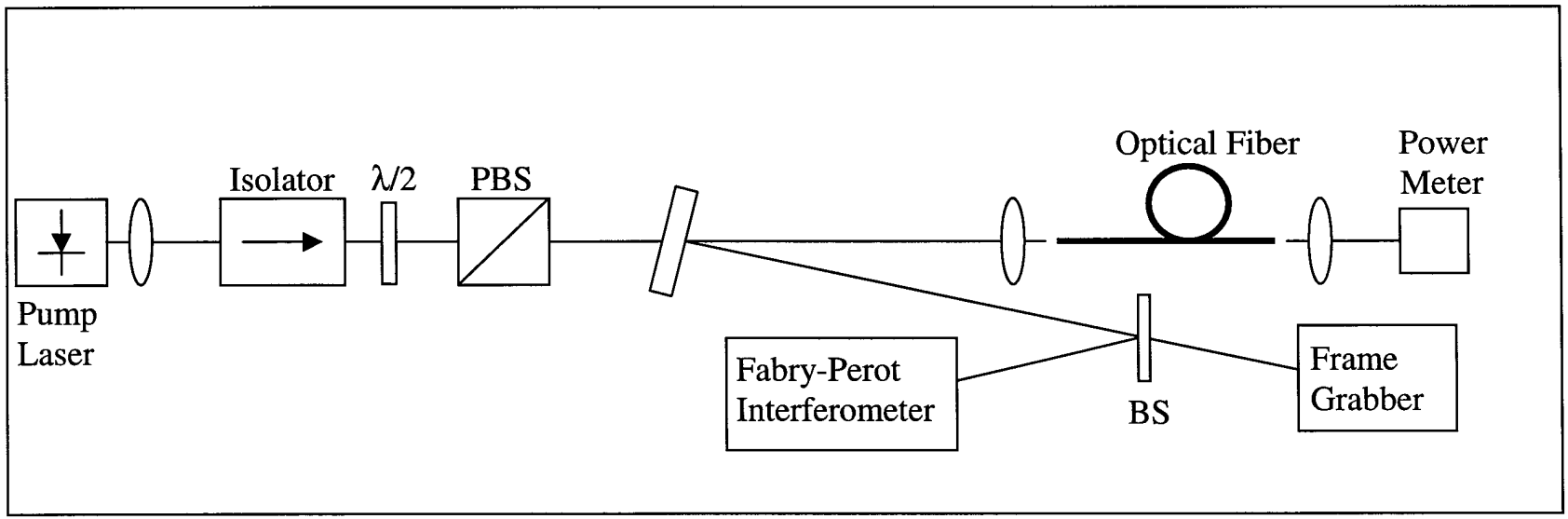

Figure 7. Experimental setup for the investigation of SBS characteristics in an optical f iber.

step-index fiber with a core mode field diameter of 9.5 μm and a numerical aperture of 0.12. The fiber length was 4.4 km. Although the fiber was a single-mode fiber at 1.3 μm, it was actually multi-mode for the wavelength of 808 nm. According to Equation 4, the fiber supports no more than 10 modes at 808 nm. According to the manufacturer's specifications, the loss in the fiber was approximately 2.2 dB/km for a wavelength of 808 nm. The fiber was held in place with an optical fiber mount that had 5 degrees of freedom.

The loss was determined experimentally using the equation below

$$P(L) = C_0 P(0) \exp(-\alpha L) \tag{28}$$

where P(0) is the power entering the coupling objective lens, L is the length of the fiber, and P(L) is the power exiting the fiber. The coupling efficiency, C_0, was determined as discussed in Chapter II by measuring the power exiting a two meter fiber. By measuring the power transmitted by the fiber as a function of input power and using Equation 28, the fiber loss, α, can be determined. The input power was kept lower than the SBS threshold power for this measurement. A Fabry-Perot Interferometer was used to monitor the backscattered light to ensure that no SBS occurred.

To determine the SBS threshold power, the SBS power was monitored by measuring the power reflected by a glass window. Plotting the SBS power as a function of input power and determining the point at which the power increases nonlinearly yields the SBS threshold. Since the glass window was at a near normal angle, the window reflected all polarizations equally. Therefore, the SBS signal that was reflected by the glass window was the same polarization as the SBS signal exiting the fiber. The

polarization was measured by using a linear polarizer and a power meter to measure the power of the reflected SBS signal.

The intensity of the SBS signal as a function of time was measured using multiple detectors. The signal was first measured using an SGD-100A PIN diode (made by EG&G Optoelectronics) which had a response time of 5 nanoseconds. The spectrum was then analyzed using a Hewlett Packard 8591E Spectrum Analyzer and both the SGD-100A PIN diode as well as an Electro-Optics ET2010A PIN diode. The second detector had a bandwidth from 50 kHz up to 800 MHz.

The cleanup capabilities of SBS in optical fibers were determined by aberrating the input laser beam prior to the optical isolator. A microscope slide that was etched in acid was used to aberrate the beam. The laser beam was then viewed with a frame grabber and BeamCode software. The BeamCode software gave contour plots of the laser beam showing the areas of high and low intensity. Ideally the beam should be Gaussian in shape. Comparing the SBS signal to the Fresnel reflection of the input laser beam gave an indication of how well the SBS process cleaned up the input laser beam.

4.2 Single Laser Beam Experimental Setup

SBS was first investigated in the 4.4 km fiber in the single-pass setup shown in Figure 7. The laser exited the optical isolator linearly polarized 45 degrees from the vertical position. The laser polarization was then rotated back to horizontal using a half-wave plate. The half-wave plate in conjunction with a polarizing beam splitter allowed any percent of the beam to be split off from the original beam to be detected by a Fabry-Perot Interferometer or a wavemeter. The glass window acted as a 7.5 percent reflector to allow power measurements of the SBS signal. A 10X objective lens was used to

couple the laser beam into the fiber giving an average coupling efficiency of 55%. The error in the coupling efficiency was estimated to be 2%.

SBS was also investigated in the 4.4 km fiber using the ring cavity setup shown in Figure 8. The ring setup is similar to the setup discussed above, however, a glass window was placed in the beam prior to the 10X objective to provide feedback to the rear end of the fiber. A 10X objective was used on the rear end of the fiber to couple the SBS light into the fiber.

4.3 Laser Beam Combination Experimental Setup

The combination of laser beams via SBS in optical fibers was also investigated. Two different experimental setups were used to determine the effectiveness of this approach. The first experimental setup, which used 2 lasers, is shown in Figure 9. Using two half-wave plates, the polarizations of the lasers were set perpendicular to each other allowing the two beams to be guided down the same path into the fiber. As in the previous experimental setup, a glass window was inserted into the beam between the polarizing beam splitter and the 10X coupling objective. The glass window was oriented at a near normal angle so that all polarizations were reflected equally. The SBS signal could be monitored by measuring the reflected signal with a power meter. A wavemeter was used to determine the wavelength of each laser. Once the laser frequencies were within 8 GHz of each other, the wavemeter was replaced by a Fabry-Perot Interferometer to match the wavelengths exactly.

The second experimental setup used for the laser beam combination investigation is shown in Figure 10. This setup consisted of only one laser beam that was split and then recombined. The beam was split using a beam splitter. Thirty-six percent of the

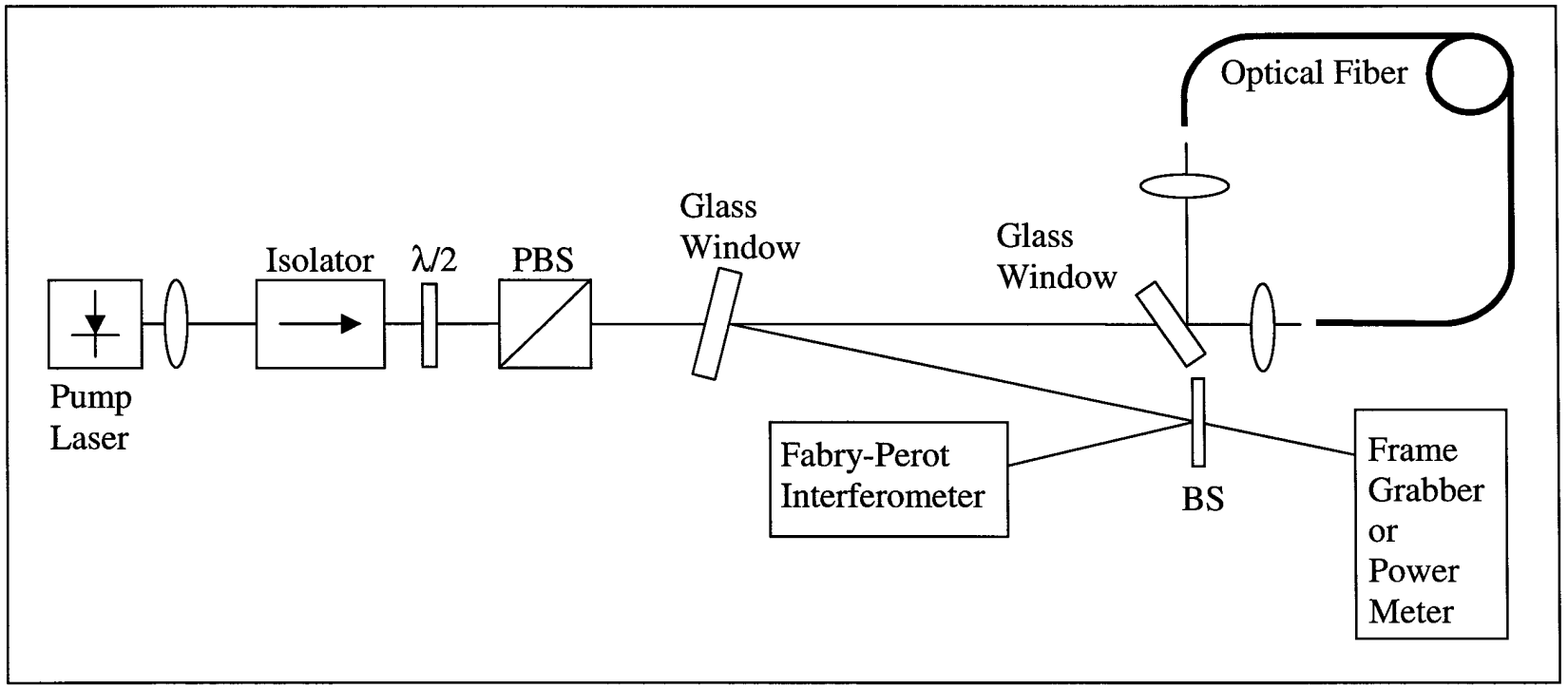

Figure 8. Experimental setup for the investigation of SBS characteristics in an optical fiber ring.

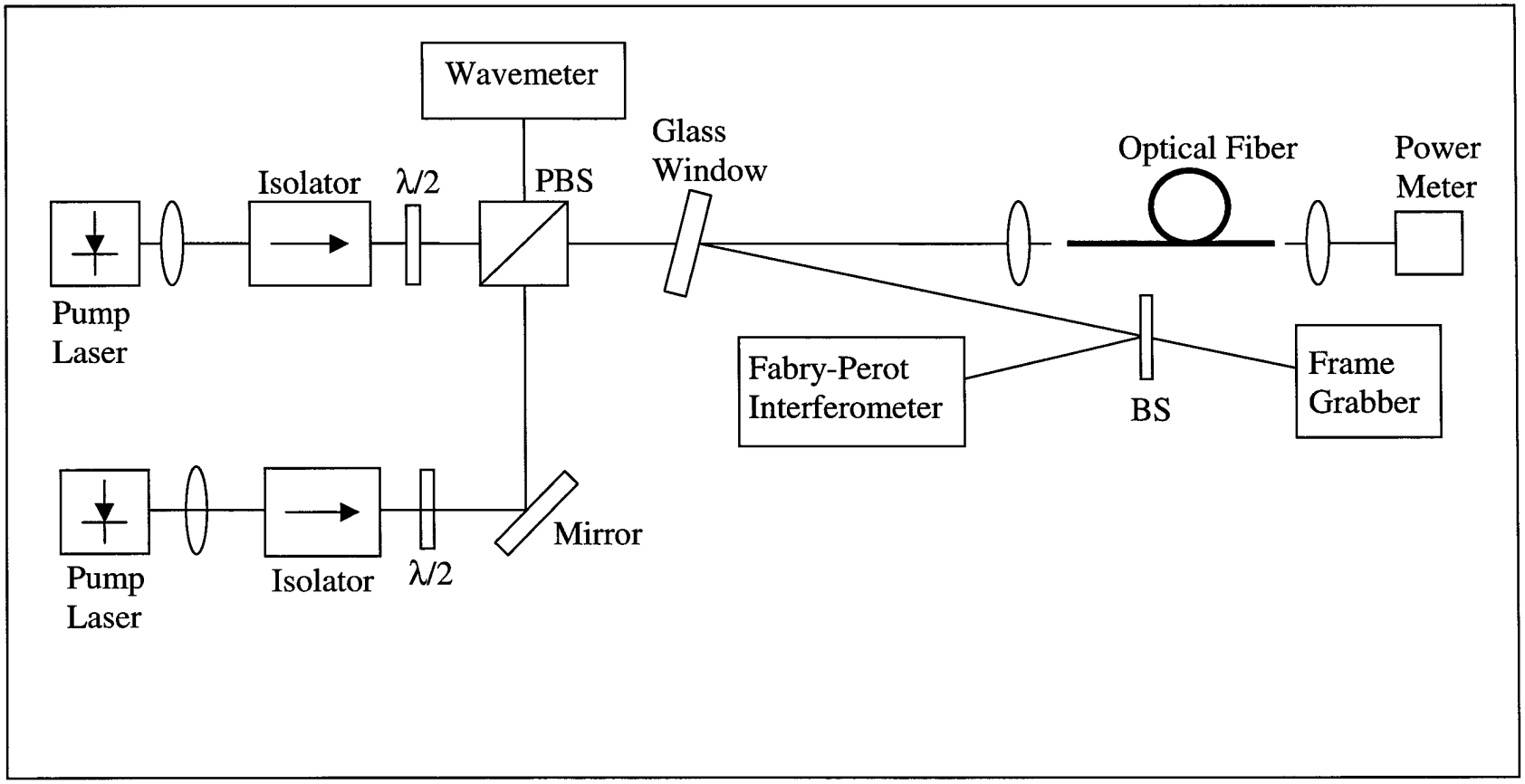

Figure 9. Experimental setup for the combination of two laser beams using SBS in an optical fiber.

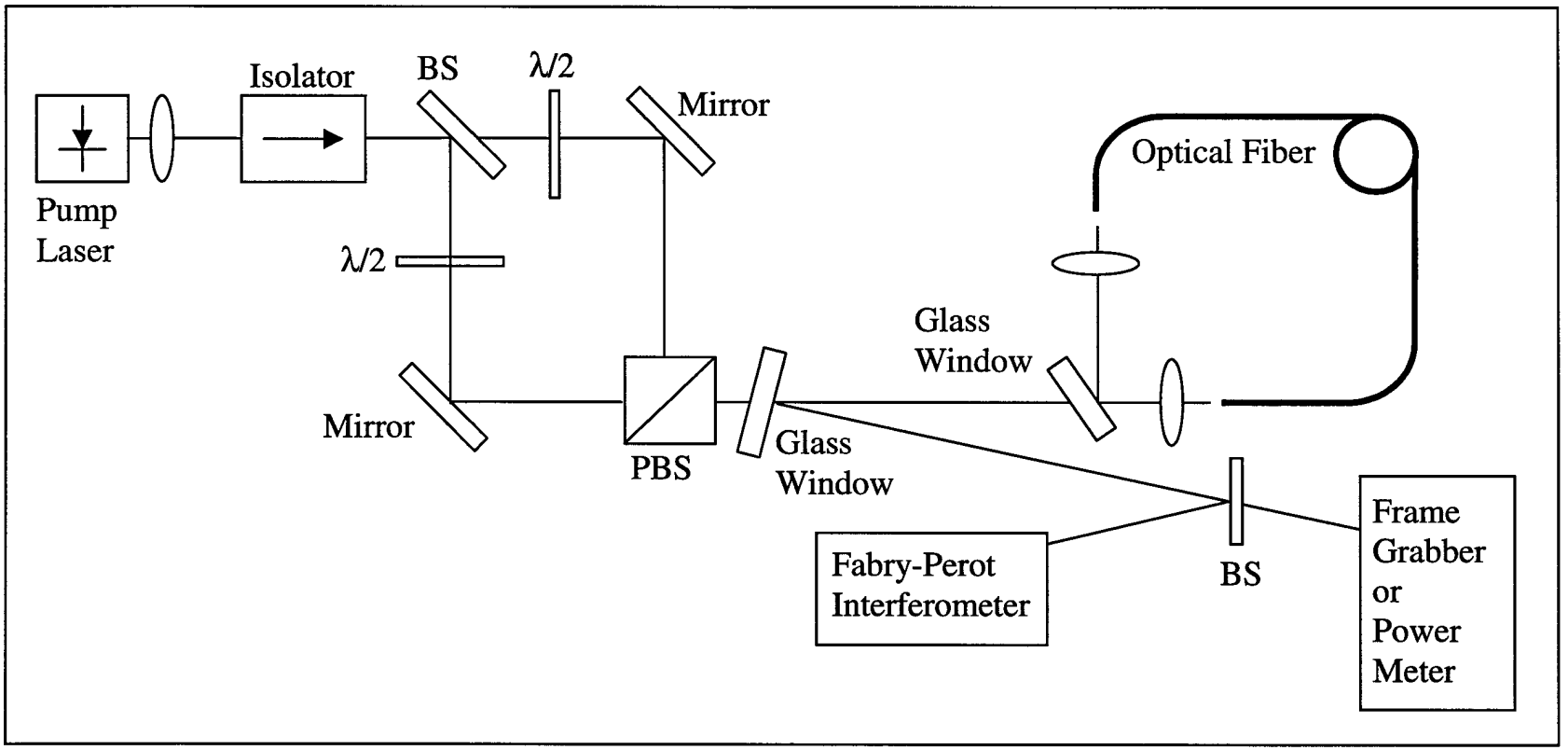

Figure 10. Experimental setup for the recombination of two laser beams using SBS in an optical fiber.

beam was redirected while sixty-four percent of the beam continued along its original path. The polarization of the two beams were then set perpendicular to each other as in the two laser case. The beams were guided along the same path using a polarizing beam splitter. Again a glass window was used to monitor the SBS output of the fiber. The two beams were coupled into the fiber using a 10X objective lens. A second glass window was used to redirect approximately four percent of the SBS beam back into the end of the fiber creating a ring. A beam stop was placed in the path of the four percent SBS beam to investigate the single- pass case. The SBS power could be monitored at either power meter shown in Figure 10.

To more accurately determine the beam combination ability of the SBS process in the fiber, a beam-in-a-bucket experiment was performed for the single laser two-beam SBS process. The experiment involved measuring the power of the SBS signal with and without an aperture in front of the power meter. The diameter of the adjustable aperture opening was adjusted to equal the spot size as measured by the frame grabber. The power of the Fresnel reflection was subtracted from the SBS power measured so that it had no effect on the measurement. The ratio of the power with the aperture closed to the power with the aperture open gives a good estimate of the quality of the combined beam. For a perfect Gaussian beam where the spot size, as measured by the frame grabber, is measured at the exp(-2) point, the beam-in-a-bucket should result in a ratio of 0.955.

4.4 Gain Measurement Experimental Setup

The fiber gain coefficients for both SBS and SRS were measured in a Corning multi-mode step-index silica core fiber with a core diameter of 50 μm and a numerical aperture of 0.2. The fiber length was 4.4 km. The experimental setup for measuring the

SBS gain coefficient is shown in Figure 11. Two lasers were used for this experiment. For the SBS gain measurement the lasers had wavelengths of 807 nm and 808 nm and were tuned by adjusting the current and temperature. The wavenumber of the Stokes laser had to be approximately 0.68 cm^{-1} less than the wavenumber of the pump laser to see any gain in the Stokes laser beam. The wavenumbers of the two lasers were monitored one at a time with the wavemeter. The power of the Stokes beam exiting the fiber was measured using a glass window inserted between the polarizing beam splitter and the coupling lens as shown in Figure 11. As the pump wavenumber was changed by increasing or decreasing the current on the laser, the Stokes power was measured. To get a more accurate measurement of the gain spectrum, the wavemeter was replaced with a Fabry-Perot Interferometer. The difference in the two laser wavenumbers can be measured with higher precision using the interferometer connected to an oscilloscope. Plotting the power as a function of the difference in wavenumber yields the gain spectrum, from which a peak value for the gain coefficient can be determined by solving Equations 13 and 14 numerically using a Runge-Kutta routine.

To measure the SRS gain coefficient, a different pair of lasers had to be used. The peak gain from SRS in silica fibers occurs for a shift of approximately 440 cm^{-1}. As shown in Figure 5, there is a secondary peak at approximately 400 cm^{-1}. For this experiment, the 808 nm laser from the SBS gain measurement was replaced with the 831 nm wavelength laser. The two lasers were tuned to have a separation in wavenumber of approximately 400 cm^{-1}. The experimental setup is shown in Figure 12. The setup was similar to that of the SBS gain measurement, however, a Stanford Research Systems SR510 lock-in amplifier had to be used to measure the gain in the Stokes signal since the

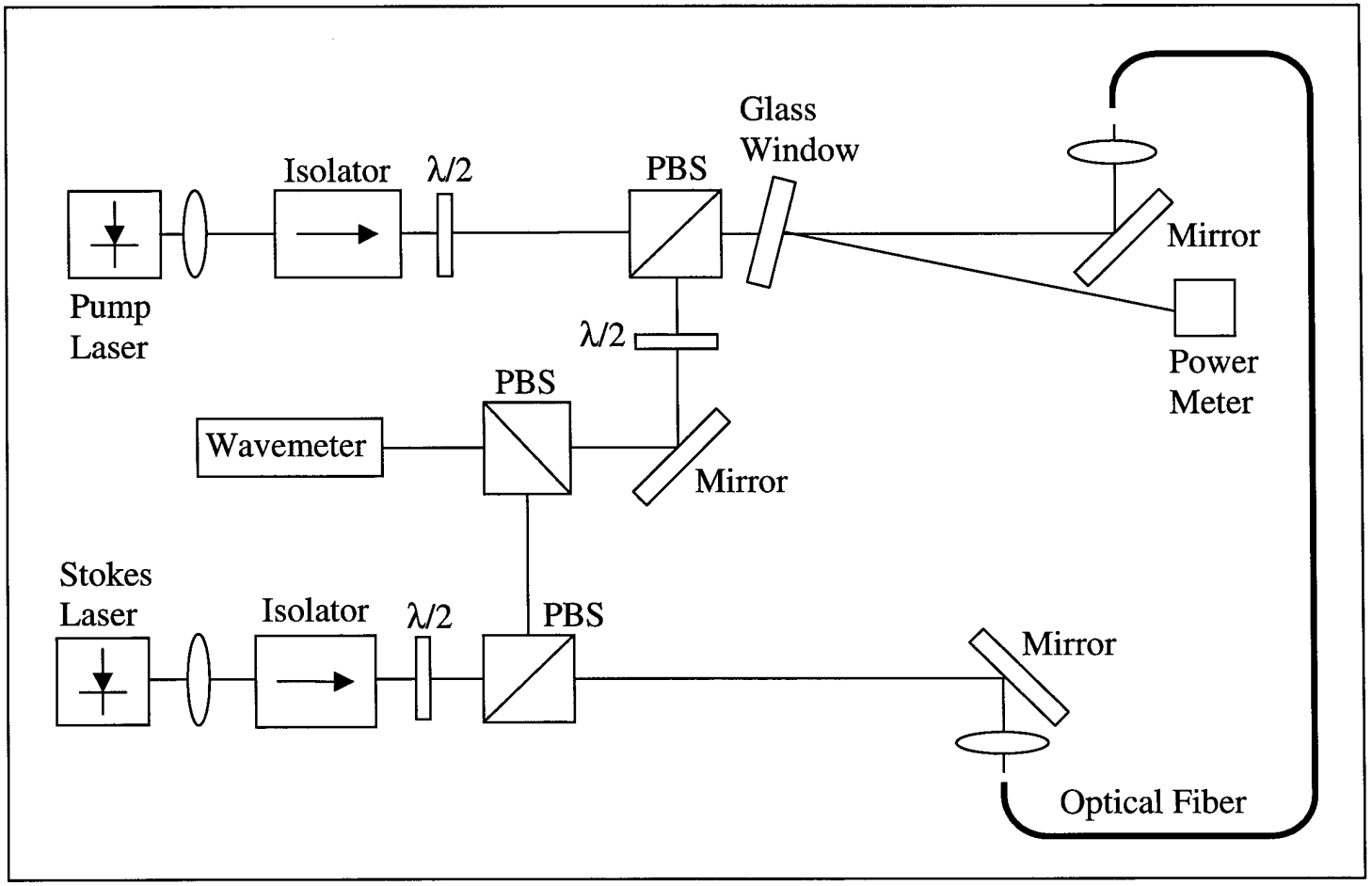

Figure 11. Experimental setup for the fiber SBS gain coefficient measurement.

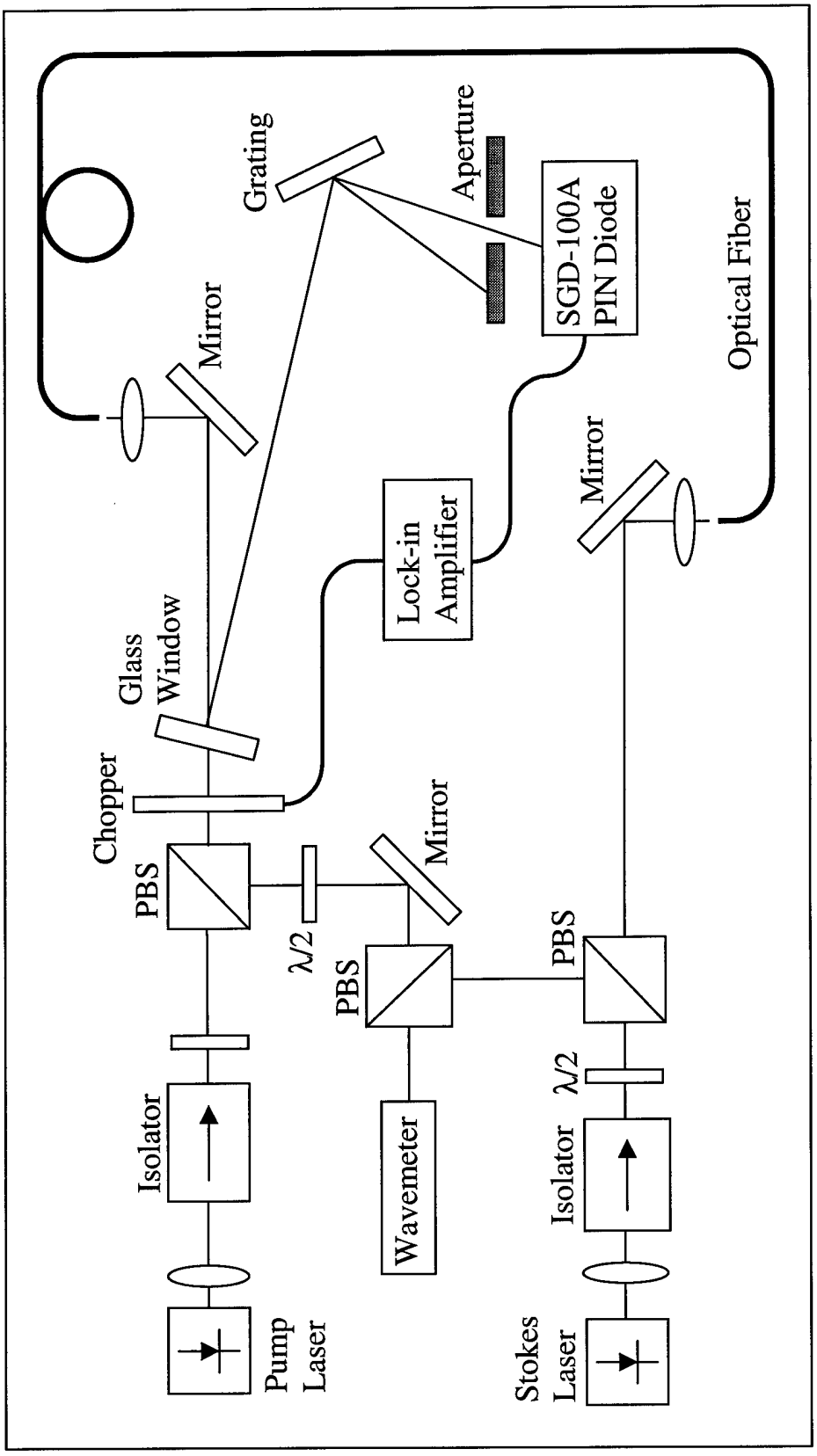

Figure 12. Experimental setup for the SRS gain coefficient measurement.

Raman gain coefficient is typically smaller than the SBS gain coefficient by two orders of magnitude. A chopper was used with the lock-in amplifier to chop the pump signal at a frequency of 1 kHz. The use of the lock-in amplifier necessitated the use of a grating and an aperture to separate the pump and Stokes beams before detecting the Stokes beam with the SGD-100A PIN diode. The lock-in amplifier gives the gain in volts instead of watts so a calibration value had to be determined to calculate the Raman gain coefficient. The calibration factor was determined using the Stokes laser and the chopper. The Stokes laser was set at its lowest detectable transmitted power. The power transmitted by the fiber was measured. The chopper was then turned on and the power measured by the lock-in amplifier. The calibration factor was then simply the ratio of the power measured in watts to the power measured in volts. The calibration factor was multiplied by the gain measured by the lock-in amplifier to give the gain in watts.

V. Results and Analysis

This chapter presents the experimental results for the various experimental setups described in Chapter IV. The chapter is separated into the results for the single-pass single beam setup, the single-pass fiber ring setup, the laser beam combining experiment, and the fiber gain coefficient measurement.

5.1 Results of SBS investigation in a single-pass setup

This section presents the results of the single-pass SBS investigation. In the single-pass setup, the characteristics of the SBS signal investigated were the SBS polarization, the SBS power threshold, the SBS power as a function of input power, the SBS intensity as a function of time, the SBS wavelength, the effect of placing a quarter wave plate in the laser beam prior to the coupling lens, and the SBS beam cleanup effects.

The SBS signal exiting the fiber was polarized horizontally similar to the input laser beam. A plot of the SBS power as a function of input power can be seen in Figure 13. The SBS power was measured by measuring the power that was reflected by the glass window and dividing by the reflectivity which had been previously determined. The power reflected by the front of the fiber can be subtracted to give just the SBS power. The SBS power threshold was determined to be 26.5 ± 0.5 mW. The threshold power was measured at the point of intersection of the linear fit to the SBS curve with the horizontal axis. Using Equation 19, the expected threshold power was calculated to be 17.5 mW. The difference could be a result of partial depolarization of the pump beam in the fiber, an error in estimating the coupling efficiency or an SBS gain coefficient different than the commonly accepted value.

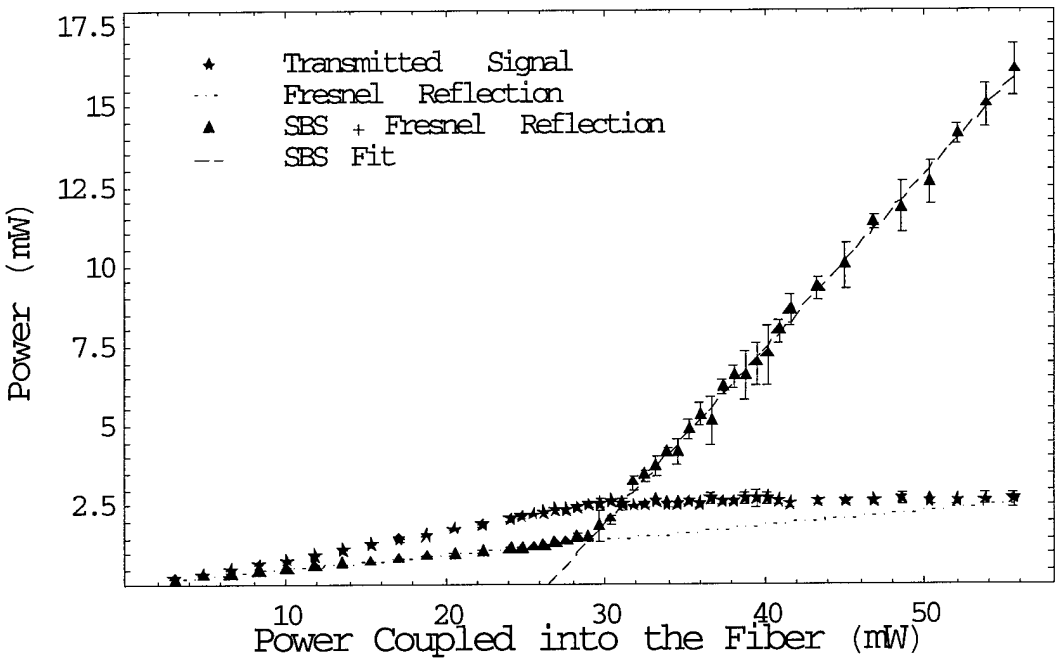

Figure 13. SBS and transmitted power vs. power coupled into the fiber in a single-pass setup.

The maximum SBS power achieved depended on the power coupled into the fiber. The coupling efficiency for the case shown in Figure 13 was 0.54 giving a maximum SBS power achieved of 13.5 mW. The best coupling efficiency achieved was 0.63, giving a maximum SBS power achieved of 21.8 mW. The SBS power conversion efficiency was 42% for the system, where the efficiency is given as the slope of the SBS power vs. input power (power measured in front of the coupling lens).

The SBS signal frequency was down shifted from the laser wavelength as expected. This is shown in Figure 14. The shift was found to be 19.20 ± 0.80 GHz. The shift was determined by measuring the shift from the laser on the Fabry-Perot Interferometer, which had a free spectral range of 8 GHz. The measured shift was then added to an integer multiple of the free spectral range of the interferometer. The multiple

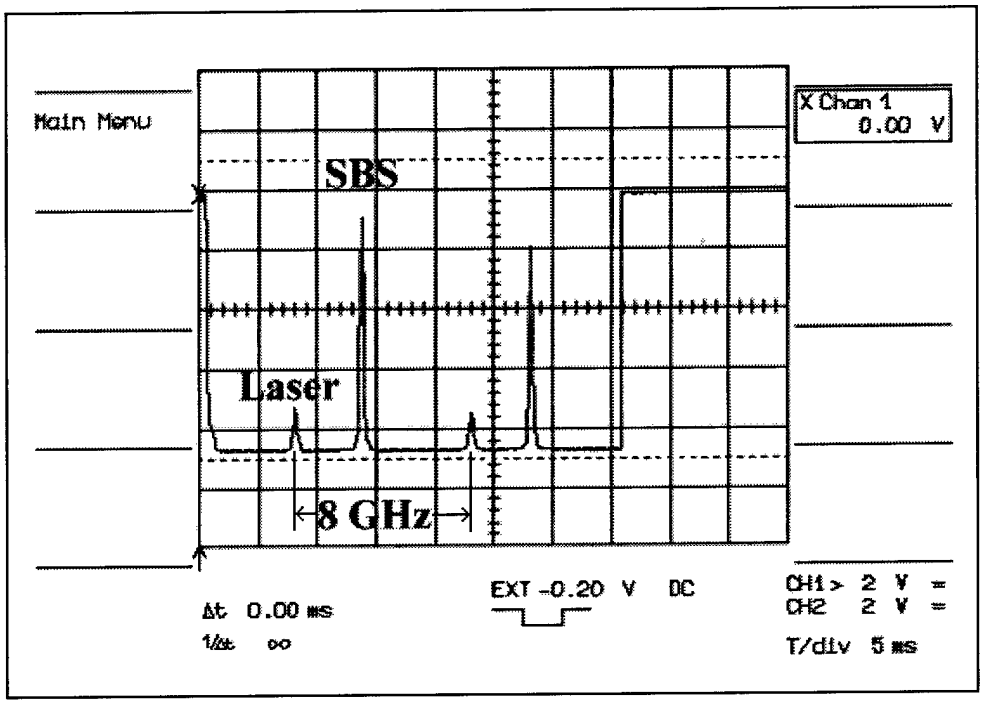

Figure 14. Fabry-Perot Interferometer output showing the SBS signal and the laser beam.

was determined by calculating the theoretical shift and picking the multiple that provided the experimental shift that was the closest to the theoretical value. The theoretical value was calculated to be 21.39 GHz. A more accurate method would have been to measure both the laser wavelength and the SBS wavelength using a wavemeter to determine the multiple of the interferometer's free spectral range. Then use the interferometer's higher resolution to accurately measure the shift between the SBS signal and the laser. This method could not be used because the wavemeter could not handle more than 30 percent amplitude noise in the signal and the SBS signal was very erratic.

The effect of adding a quarter-wave plate between the coupling lens and the glass window in the experimental setup shown in Figure 7 was also investigated. The quarter wave plate was rotated so that the optical axis was 45 degrees from the laser beam

polarization. The quarter wave plate converts the linearly polarized laser beam to circular polarization. It was expected that the SBS light would be circularly polarized in the opposite direction similar to the light reflected off of the fiber end. The experiment showed, however, that this was not the case. After passing back through the quarter wave plate, the SBS light was linearly polarized in the same direction as the input laser beam.

As mentioned previously, the SBS signal amplitude fluctuated more than 30 percent from the mean. This can be seen in the real time oscilloscope trace of the SBS signal intensity shown in Figure 15. An expanded view of the SBS signal is also shown in Figure 15. Figures 16a through 16c are representative of the many traces taken for the single-pass case as the laser power was increased. From a comparison of Figures 16a

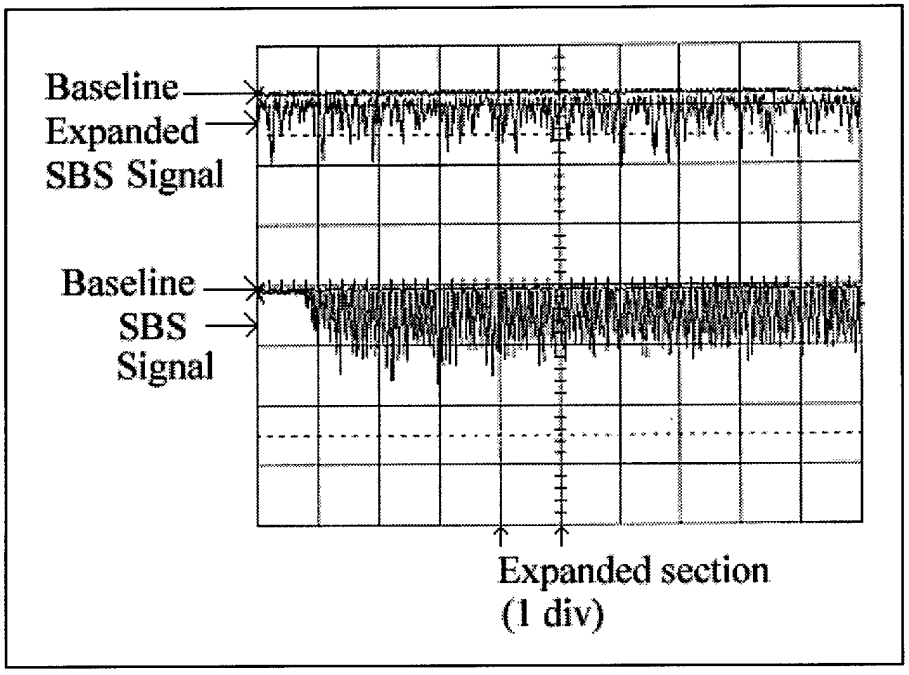

Figure 15. SBS intensity real time oscilloscope trace (50 μsec/div) and an expanded view (5 μsec/div) of the SBS signal for the single-pass setup with 40 mW of input power. Top trace shows an expanded view of the section between the two arrows.

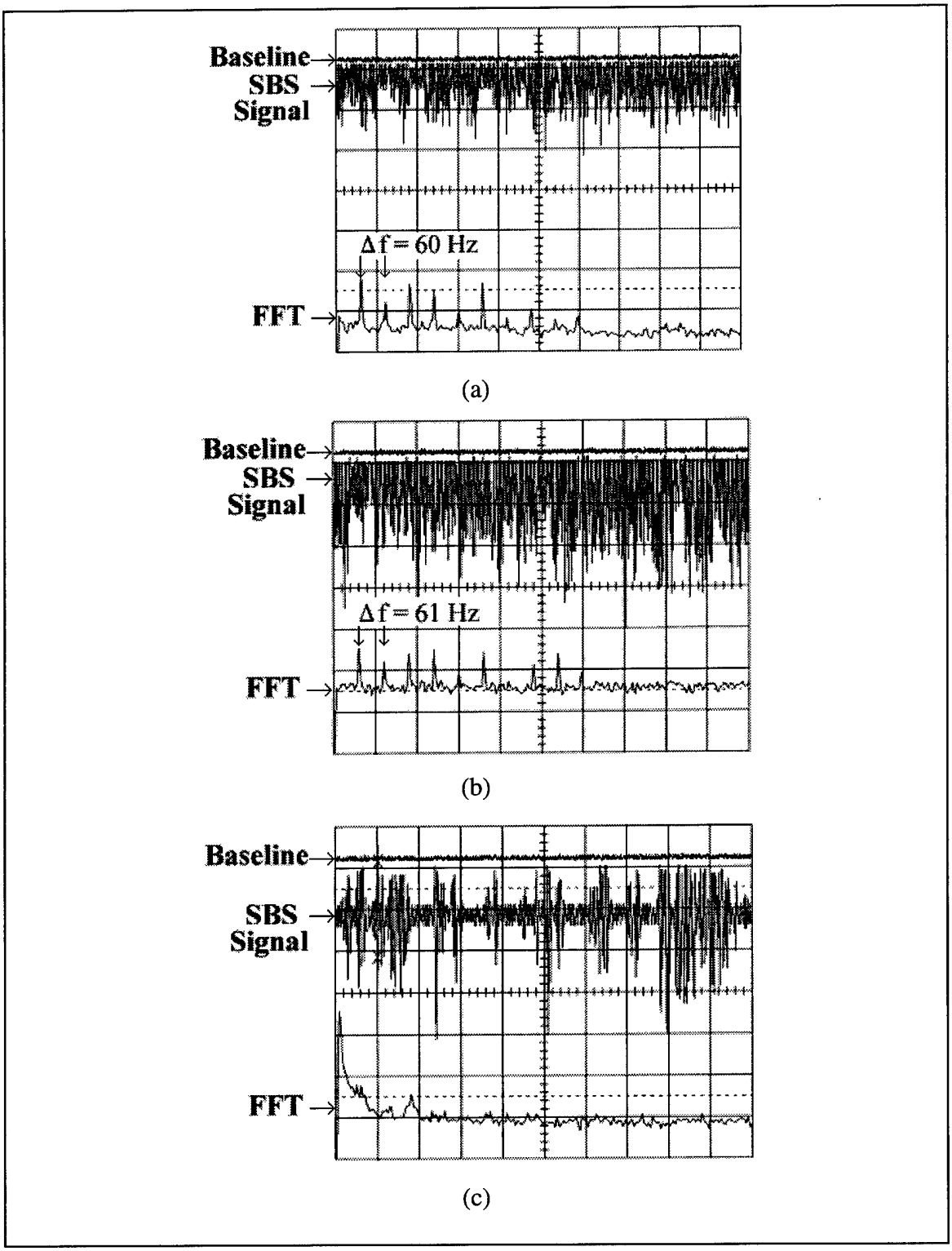

Figure 16. SBS intensity real time oscilloscope trace (20 msec/div, 50 Hz/div) for the single-pass setup with (a) 36 mW input power (b) 48 mW input power (c) 66 mW input power.

through 16c, it can be seen that the SBS signal behavior initially fluctuated more as the power was increased. As the power was increased further, however, the SBS signal became more constant, as can be seen in Figure 16c. Figure 4 shows that the SBS signal should become a steady signal when the ratio of the SBS intensity to the pump intensity at the front of the fiber, b_0, is greater than 0.7 and the gain factor, g_0L, is greater than 20 [9]. For Figure 16c, the laser was at maximum power giving a gain factor of 205 and a b_0 of 0.47. Therefore, the SBS signal should be unstable, as was seen. Once the input power is increased to give an SBS signal power of 70 percent of the input signal, the SBS signal is expected to become stable. This could not be observed because of the power limitations of the laser used. Figure 16c shows the SBS signal at the maximum possible input power given the pump laser power constraints.

The bottom signal shown in each of the three images in Figure 16 is the power-averaged fast Fourier transform (FFT) of the SBS signal. The FFT signals shown in Figure 16 show a few frequencies, which do not correspond to anything physical. The 60 Hz frequency shown in Figure 16a and Figure 16b is most likely a result of much of the equipment running on 60 Hz AC power. The other spikes shown are simply noise. Figure 17 shows the SBS signal on a smaller time scale per division. The FFT in Figure 17 shows a frequency of 23.25 kHz for this particular trace. The mean frequency for all of the traces was found to be 22.25 ± 0.65 kHz. This corresponds to twice the photon transit time down the length of the fiber. The expected frequency for the 4.4 km fiber was 23.51 kHz. For a better determination of the frequencies in the SBS spectrum, a spectrum analyzer was also used with the SGD-100A PIN diode. The spectrum of the SBS signal is shown in Figure 18. Figure 18 shows a frequency of oscillation in the SBS

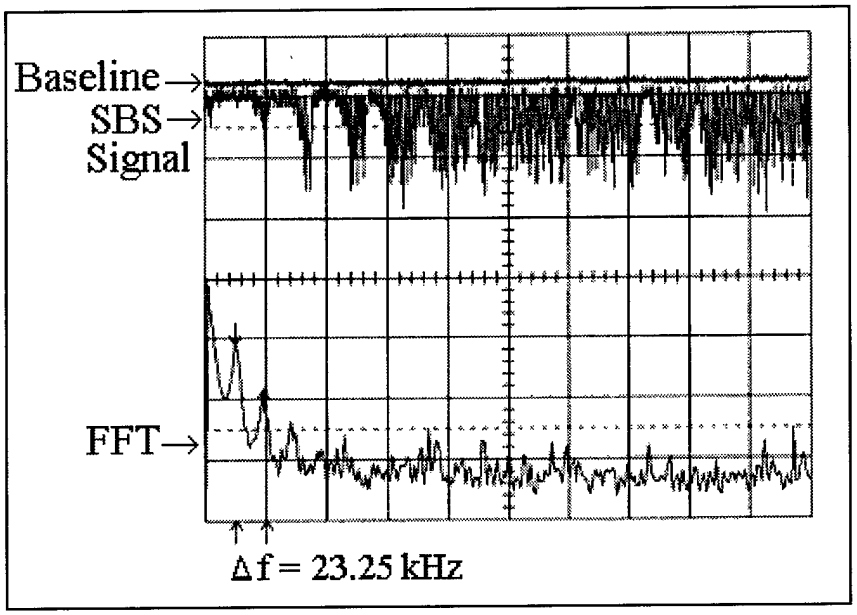

Figure 17. SBS intensity real-time oscilloscope trace (50 μsec/div) showing a 23.25 kHz oscillation for the single-pass setup with 36 mW of input power.

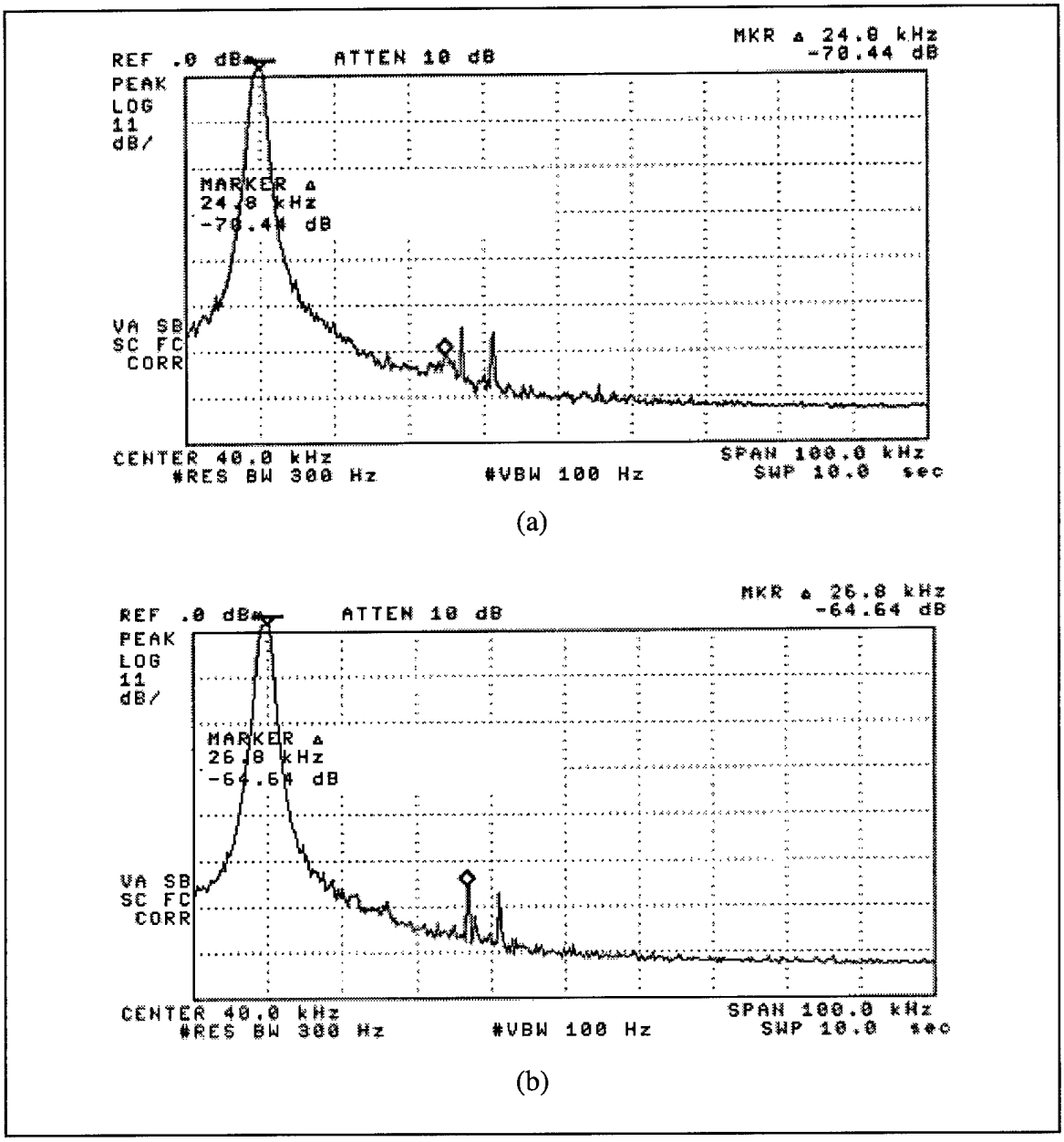

Figure 18. SBS RF Spectrum (100 kHz span) for the single-pass setup with 51 mW of input power. (a) SBS spectrum, (b) spectrum for no signal.

signal of 24.8 kHz. Figure 18a must be compared to Figure 18b to see that the three most prominent peaks in the spectrum are meaningless since they are present without any signal.

While it is clear that there is some oscillation in the SBS signal corresponding to twice the photon transit time, this does not explain all of the amplitude fluctuation in the SBS signal. While the periodicity in the largest peaks in Figure 15 can be attributed to the SBS oscillation, there are many other random amplitude fluctuations between the peaks. This is most likely attributed to the chaotic nature of SBS seen by Harrison *et al.* [15].

The beam cleanup effects of the SBS process were also investigated. The SBS signal was compared for the cases of with and without aberrating the input laser beam. The contour maps of the Fresnel reflection of the laser beam off of the fiber and the SBS signal for both the aberrated and unaberrated cases are shown in Figure 19. From Figure 19, it can be seen that the SBS signal was a very clean Gaussian shape for both the unaberrated and aberrated cases. The SBS signal did not change location over time, as the angle at which the pump beam entered the fiber was adjusted, or as the laser power was adjusted. Figure 19 shows a small change in the location of the SBS signal between the two cases. The change in location of the SBS signal is a result of the microscope slide changing the path of the input beam enough that the fiber mount had to be adjusted slightly to couple the beam into the fiber. Changing the location of the fiber in relation to the coupling lens causes slight changes in the path of the SBS beam. Using a larger diameter fiber would remove the extreme sensitivity of the fiber to pump beam path

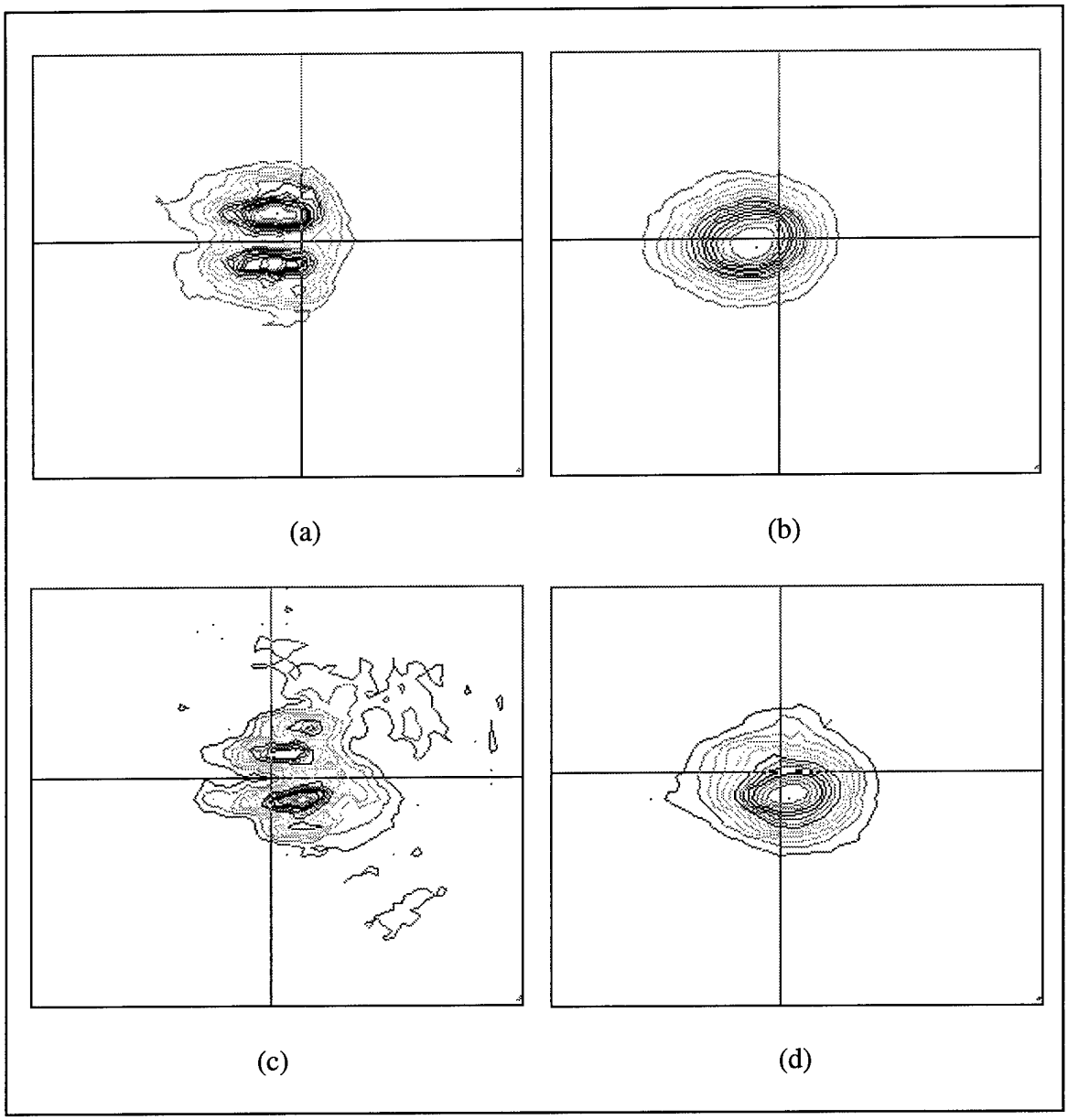

Figure 19. Contour plot of the SBS signal and the Fresnel reflection of the input laser beam for both aberrated and unaberrated beams in the single-pass setup. (a) Fresnel reflection from one input laser beam (b) SBS signal (c) Fresnel reflection from one aberrated input laser beam (d) SBS signal produced from the aberrated beam.

adjustments. The double peak structure shown in the input beam is a characteristic of the laser being used and is not caused by the optics in the system.

5.2 Results of SBS in a Fiber Ring

The threshold power for SBS in the fiber ring setup was found to be 21.0 ± 0.7 mW. A plot of the SBS power exiting the ring as a function of power input into the fiber is shown in Figure 20. The maximum achieved SBS power exiting the ring was 36.2 mW

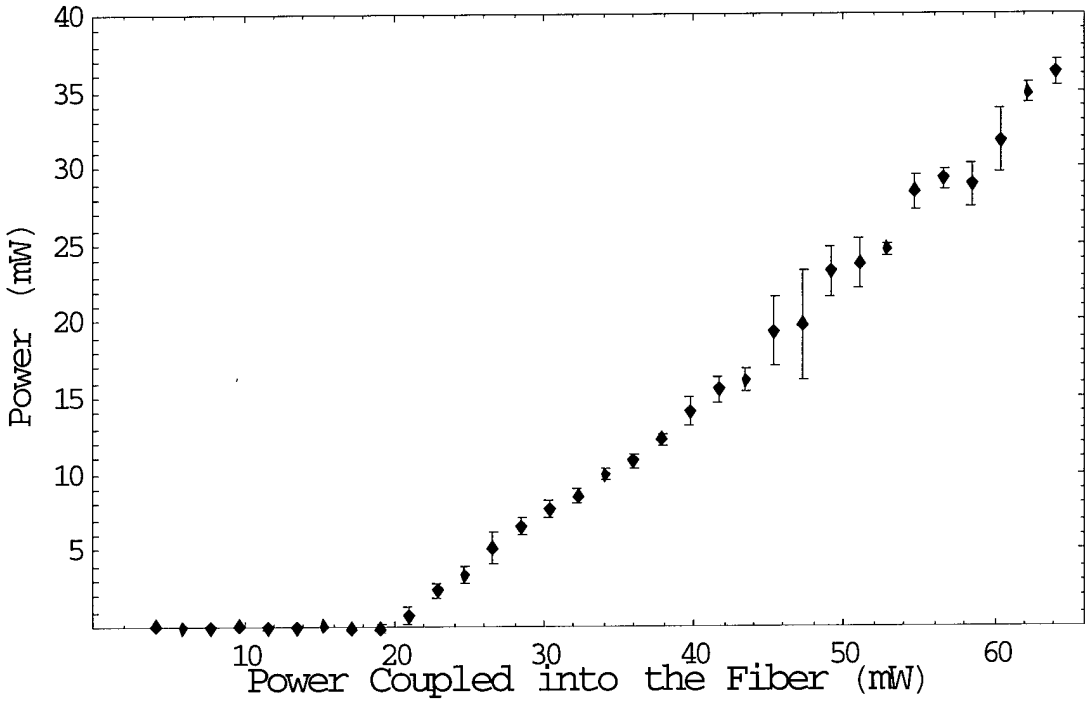

Figure 20. SBS power vs. power coupled into the fiber for the fiber ring setup.

with an SBS power conversion slope efficiency of 52%.

The SBS signal was polarized horizontally as was the input laser beam. The Stokes shift was measured to be 19.03 ± .05 GHz. This is within the experimental error of the Stokes shift measured for the single-pass case. The intensity of the SBS signal as a

function of time is shown in Figures 21 and 22. Figure 21 shows there is some periodicity in the SBS signal as was seen in the single-pass case. For the fiber ring, the

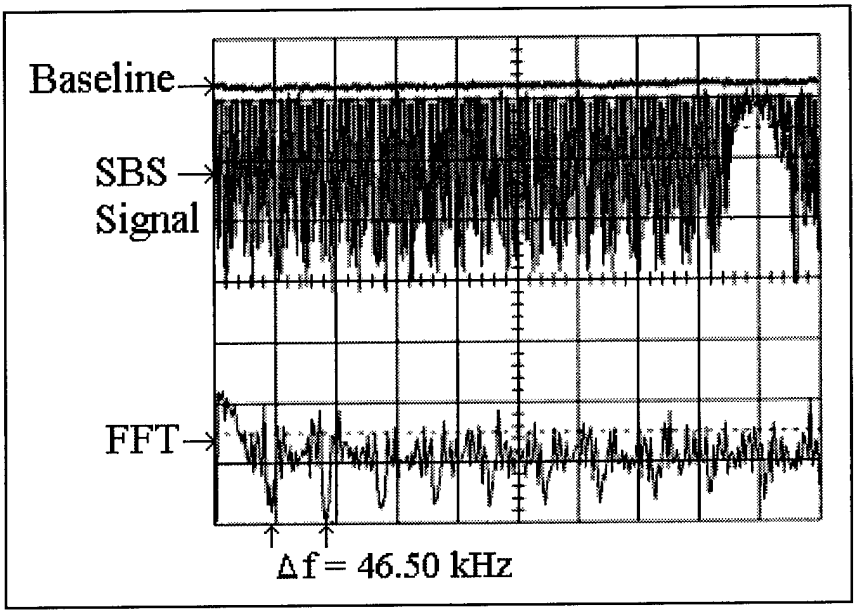

Figure 21. SBS intensity real-time oscilloscope trace (50 μsec/div) for the fiber ring setup with 48 mW of input power.

frequency was 45.45 ± 0.67 kHz. This frequency corresponds to the round-trip photon transit time around the fiber ring. It is not twice the photon transit time down the length of the fiber since the ring couples the SBS light immediately back into the other end of the fiber. This accounts for the factor of two difference between the single-pass oscillation frequency and the fiber ring oscillation frequency. The expected frequency of oscillation was 46.95 kHz.

Because the details of the SBS signal are difficult to see in the trace shown in Figure 21, Figure 22 shows the real time oscilloscope trace of the SBS signal with a zoomed in view of a portion of the signal. The top SBS signal shown in Figure 22 is one

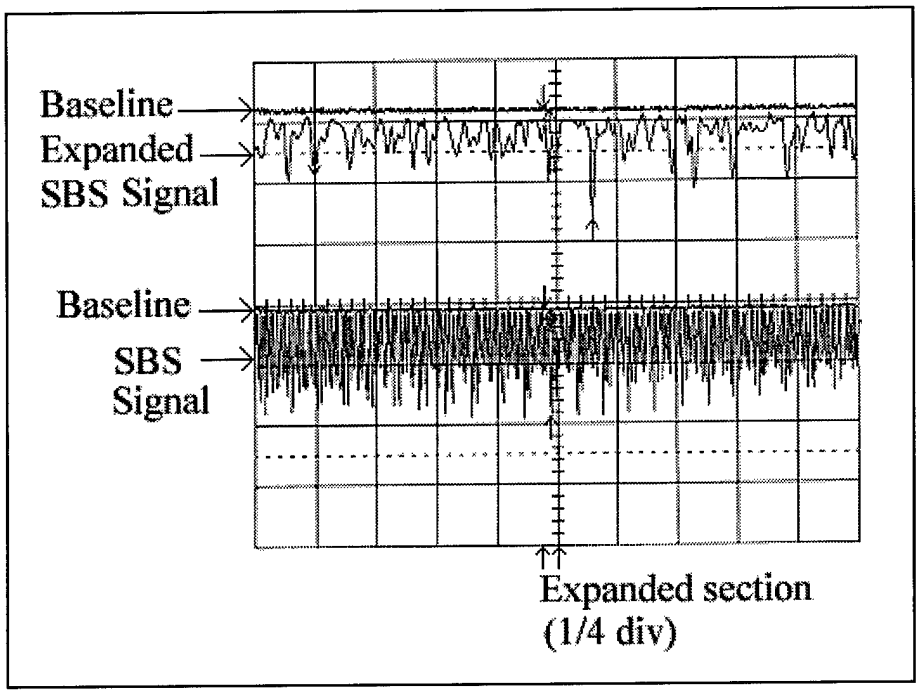

Figure 22. Expanded view (1.25 μsec/div) of the real-time oscilloscope trace (50 μsec/div) of the SBS intensity for the fiber ring setup with 46 mW of input power.

fourth of a division of the bottom SBS signal. The periodicity of the largest peaks in the SBS signal correspond to the 45.45 kHz oscillation frequency discussed above. The amplitude fluctuations between the largest peaks are most likely a result of the chaotic nature of the SBS as mentioned previously.

The traces shown in Figures 21 through 23 are representative of the many traces taken as the laser power was increased. From a comparison of Figures 23a through 23c, it can be seen that the SBS signal behavior initially fluctuated more as the power was increased. As the power was increased further above the SBS threshold, however, the SBS signal eventually began to settle down, as seen in Figure 23c. The fluctuating behavior appeared to be only a function of input power and not a function of the ring or

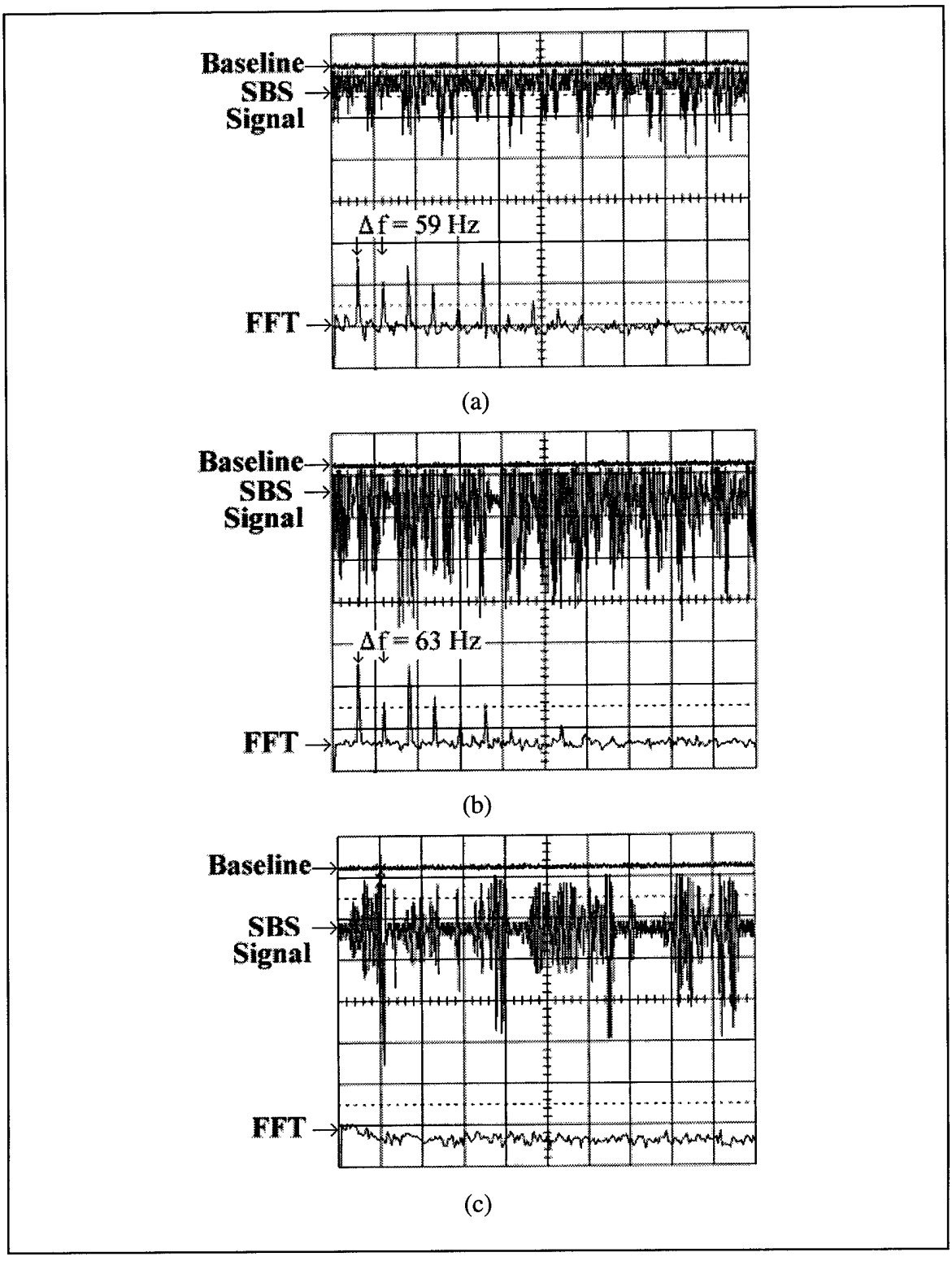

Figure 23. SBS intensity real-time oscilloscope traces (20 msec/div, 50 Hz/div) for the fiber ring setup with (a) 32 mW input power, (b) 42 mW input power, and (c) 66 mW input power.

single-pass case. The SBS intensity real time oscilloscope traces for the fiber ring were similar to traces for the single-pass case for equal SBS power levels. The major difference was in the oscillation of the SBS intensity as mentioned previously. For Figure 23c, the laser was at maximum power giving a gain factor of 202 and a b_0 of 0.55. Therefore, the SBS signal should be unstable as was seen in Figure 23c.

The SBS signal was also analyzed with the spectrum analyzer. Figures 24 and 25 show the results from the spectrum analyzer. The spectrum analyzer gave results similar to the results from the FFT of the SBS signal. An oscillation frequency of 47.4 ± 0.5 kHz was found with the spectrum analyzer. This is within the experimental error of the expected value. A frequency of 64.9 ± 1.8 MHz was also found as seen in Figure 25. This corresponds to the SBS signal exiting the front of the fiber, traveling back to the laser and disrupting it. The disrupted beam then travels to the fiber causing a lower SBS power, giving rise to the 64.9 MHz oscillation. Although an optical isolator was used, the SBS signal was still strong enough to pass through the isolator and disrupt the laser. The optical path length from the laser to the front of the fiber was 234 cm. From the round trip time between the laser and the front of the fiber, the expected frequency was 64.1 MHz. The results are within the experimental error of the theoretical results. Various harmonics of the expected 64.1 MHz frequency are also present, as shown in Figure 25. The 64.1 MHz frequency could not be seen in the single-pass case because the SBS signal was much weaker than for the ring case. To see the 64.1 MHz frequency, the SBS signal had to be strong enough that it could pass through the optical isolator and disrupt the laser, producing oscillations large enough to be seen above the noise. To test this explanation for the 64.1 MHz frequency, the polarizer on the optical isolator was

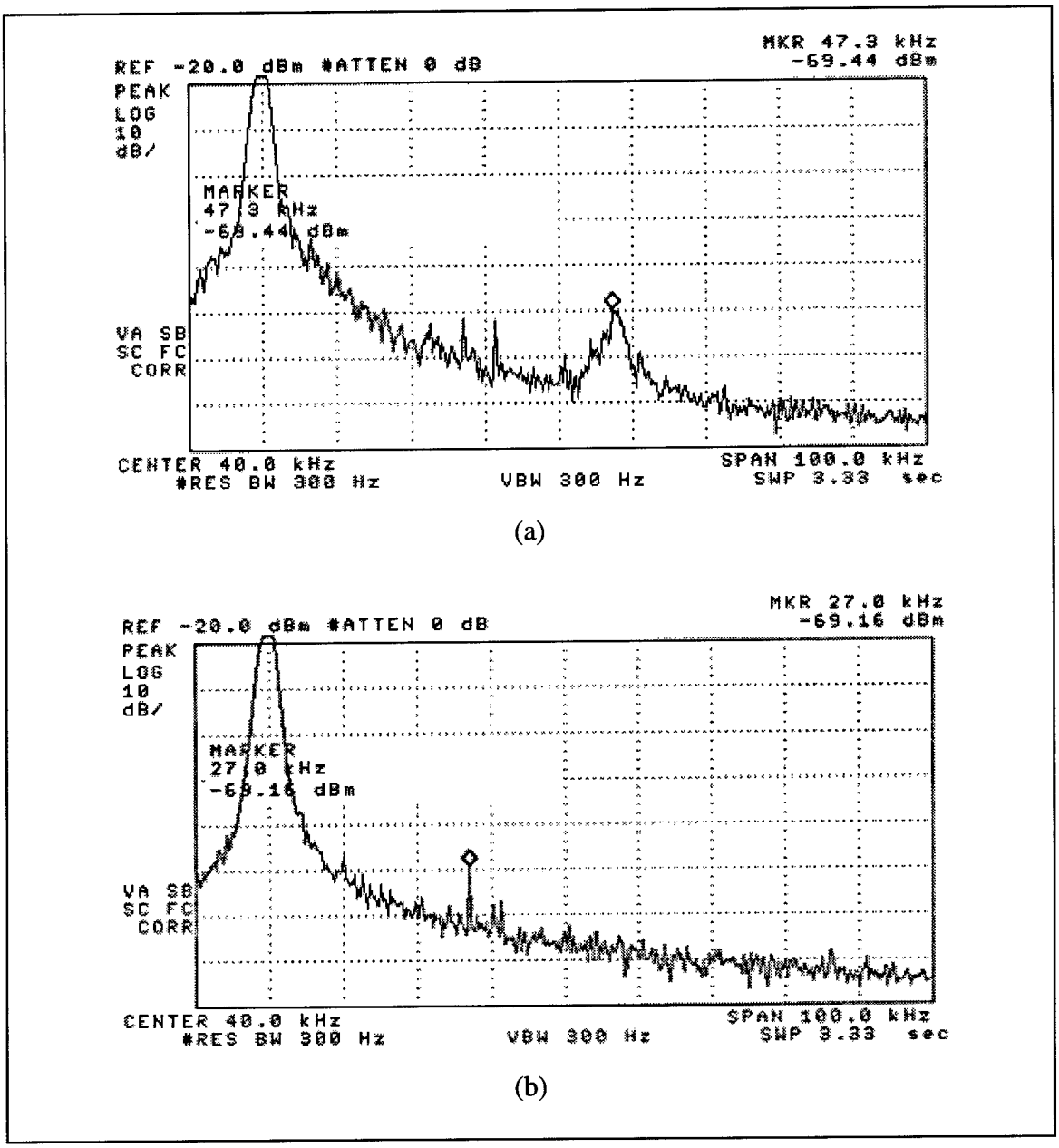

Figure 24. SBS RF spectrum (100 kHz span) for one laser beam coupled into a fiber ring with 51 mW of input power. (a) SBS RF spectrum, (b) RF spectrum for no signal.

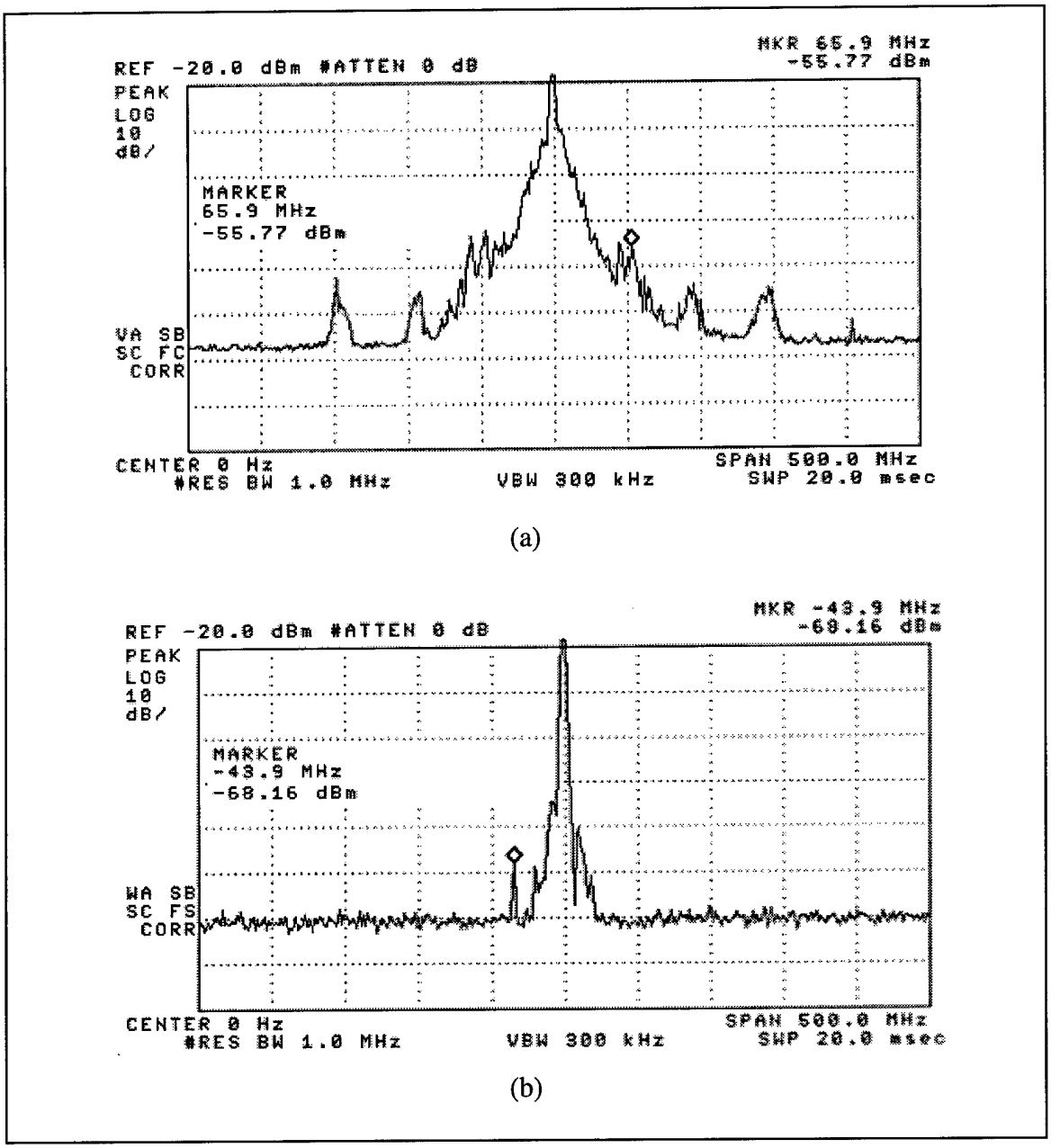

Figure 25. SBS RF spectrum (500 MHz span) for one laser beam coupled into a fiber ring with 50 mW of input power. (a) SBS RF spectrum, (b) RF spectrum for no signal.

rotated so that the effective isolation was reduced. The reduced isolation produced a stronger oscillation in the SBS signal observed on the spectrum analyzer. For the single-pass case, the SBS signal was not strong enough to pass through the optical isolator and disrupt the laser enough to produce oscillations large enough to be detected above the noise.

The fiber ring also worked well for cleaning up an aberrated laser beam. The only visible difference in the cleanup ability of the fiber ring compared with the single-pass case was the lower SBS threshold power. The lower threshold power allowed laser beams with lower input power to be cleaned up. The contour plot of the SBS signal was similar to the single-pass case. It can be seen from Figure 26 that the resulting SBS signal is a nice Gaussian shape even when the input signal is very aberrated. The double peak structure in the contour plot of the input beam is a characteristic of the laser.

5.3 Laser Beam Combining Results

The combining of two laser beams via SBS in an optical fiber was investigated with both one and two laser setups. For the two laser case shown in Figure 9, the SBS beam was extremely erratic. This is in part because of the need for the two lasers to be matched in wavenumber to within less than 0.01 cm^{-1}. Both lasers were very unstable which is not surprising since diode lasers are known to be very sensitive to feedback. Both lasers had trouble maintaining their wavelength and would typically mode hop to a different wavelength randomly every few minutes. They also would rapidly fluctuate by 0.02 to 0.03 cm^{-1}. This caused the SBS signal to be very erratic. When the two lasers were matched in wavenumber, the SBS signal could be seen with the Fabry-Perot Interferometer. The SBS signal was not present until the laser wavenumbers were

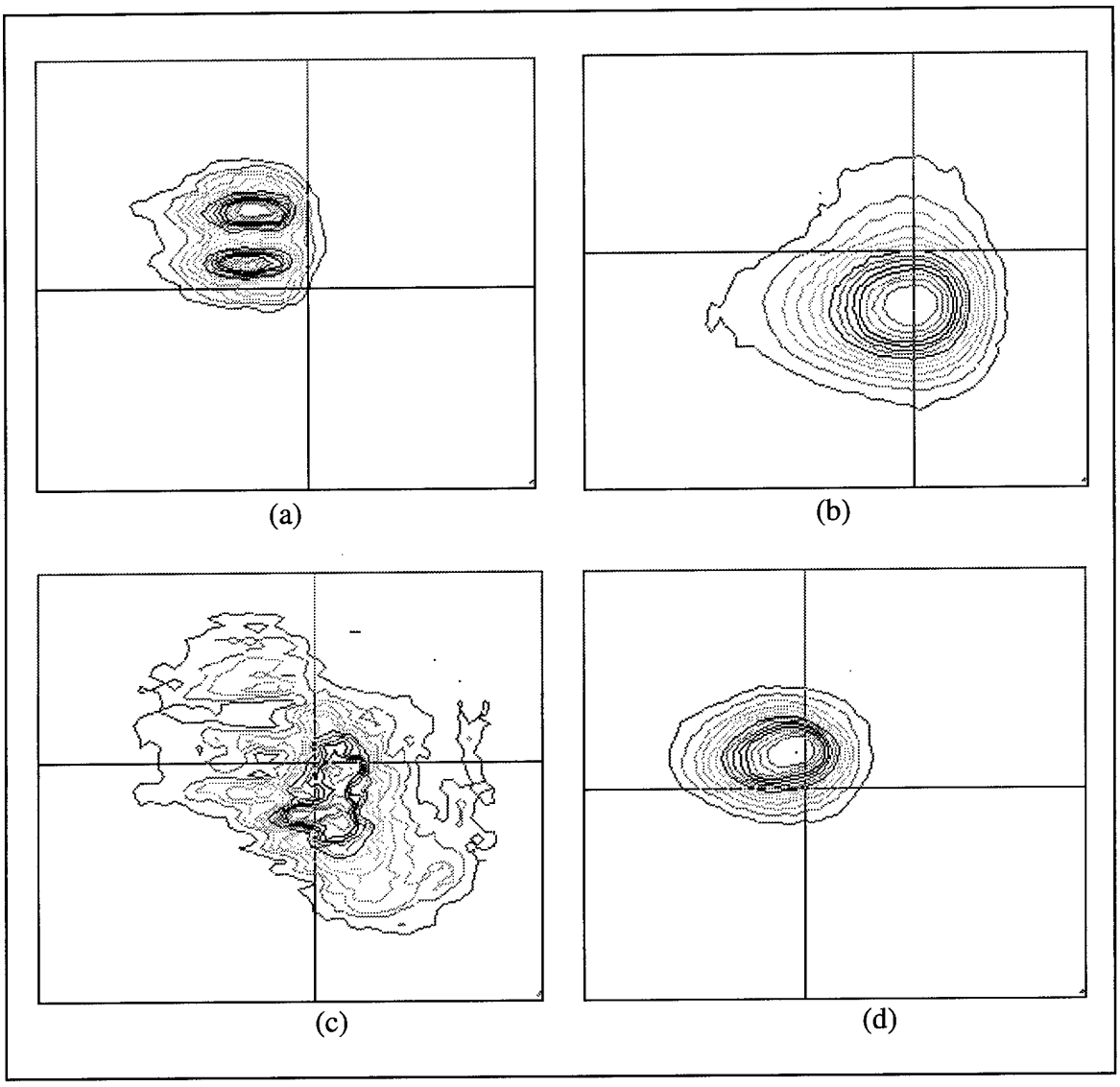

Figure 26. Contour plot of the SBS signal and the Fresnel reflection of the input laser beam for both aberrated and unaberrated beams in the fiber ring setup. (a) Unaberrated input laser beam (b) SBS and input laser beam for unaberrated case (c) Aberrated input laser beam (d) SBS and input laser beam for aberrated case.

matched within 0.01 cm^{-1}. The laser current had to be continually monitored and adjusted because of the behavior of the lasers. Since the optical isolators could not completely isolate the lasers, the feedback from the SBS signal made the mode hopping of the lasers even worse. Because of the problems caused by the fluctuations in the laser wavenumbers, it was not possible to aberrate the beam to determine if the SBS signal cleaned up the beam.

The single laser case was much more successful than the two laser case. The success of the single laser case is a result of the fact that both beams were always the same wavelength. As the laser changed wavenumber, both beams also changed allowing both beams to constantly work together to create the SBS signal. As with the single beam setup discussed previously, the fiber ring setup and the single-pass setup produced similar results. The only major difference between the two cases was the threshold power. The results of the SBS intensity real time oscilloscope traces were similar to those shown in Figures 16, 17, 21, and 23. There was no visible difference between the real time oscilloscope traces for the single beam setup and those for the two beam setup.

The SBS spectrum was also similar to the single beam case. The major difference in the spectrum was a result of being able to get a stronger SBS signal. The diode was placed in two different locations for this case. The first location was the same as the single laser case in which the SBS signal was reflected by a glass window into the detector. The second location was in line with the beam splitter. Approximately 45 percent of the SBS signal was separated from the laser beam by the beam splitter. This higher power signal allowed for the signals to be seen more clearly, especially for the single-pass case. Figures 27 and 28 show the spectrum for the single-pass case with two

beams. Figures 29 and 30 show the spectrum for the fiber ring case with two beams. For the single-pass case, a frequency of 24.7 ± 0.9 kHz was found. This is within two standard deviations of the expected value and only 0.1 kHz less than the value found by the spectrum analyzer for the single beam case. The oscillation corresponding to the round trip photon transit time between the laser and the front of the fiber was also found. The distance between the laser and the fiber end was 258 cm. This gave an expected oscillation of 58.1 MHz. The actual oscillation was 57.5 ± 1.3 MHz, which is within the experimental error of the expected value.

For the fiber ring case, the results were similar to the single beam fiber ring case. Using the spectrum analyzer, the oscillation frequency corresponding to the photon transit time around the fiber ring was found to be 48.4 ± 1.3 kHz. This is within the experimental error of the single beam, fiber ring oscillation frequency. The frequency corresponding to the round trip photon transit time between the laser and the front of the fiber was found to be 54.1 ± 1.9 MHz. Both oscillation frequencies were as expected and similar to the single beam case. The two beams did not have an effect on the SBS oscillations when compared to the single beam fiber ring case. The SBS amplitude fluctuations for the two beam case were similar to the single beam case.

Figure 31 shows the SBS signal with the laser at its maximum power. Both Figures 30 and 31 show that the SBS signal was very erratic. As the SBS signal became stronger, the amplitude fluctuations could more easily be detected above the noise. The frequency corresponding to the round trip transit time between the laser and the front of the fiber and its harmonics were always present, but the other frequencies seen in Figure

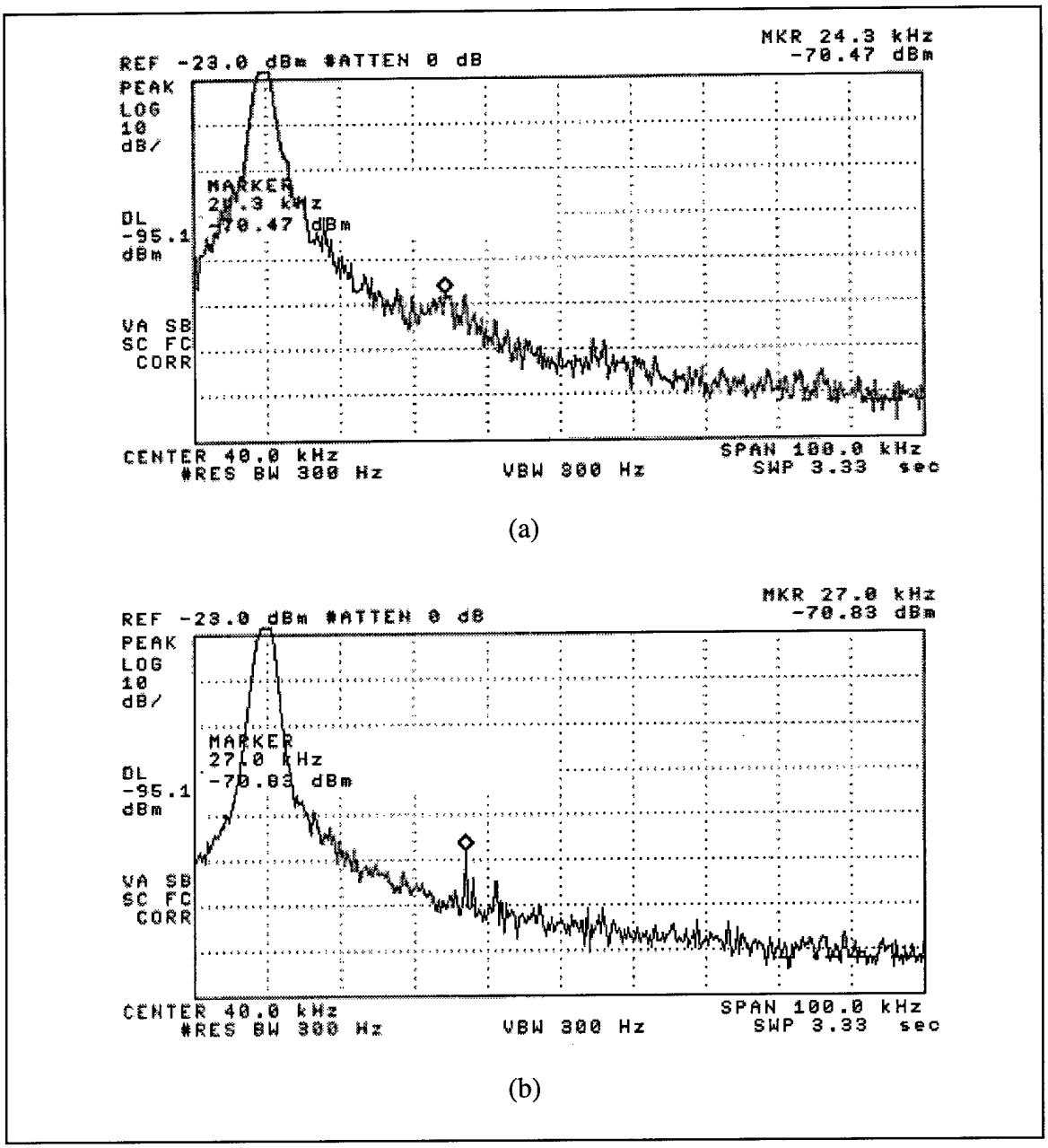

Figure 27. SBS RF spectrum (100 kHz span) for two laser beams coupled into a single-pass setup with 40 mW of input power. (a) SBS RF spectrum, (b) RF spectrum for no signal.

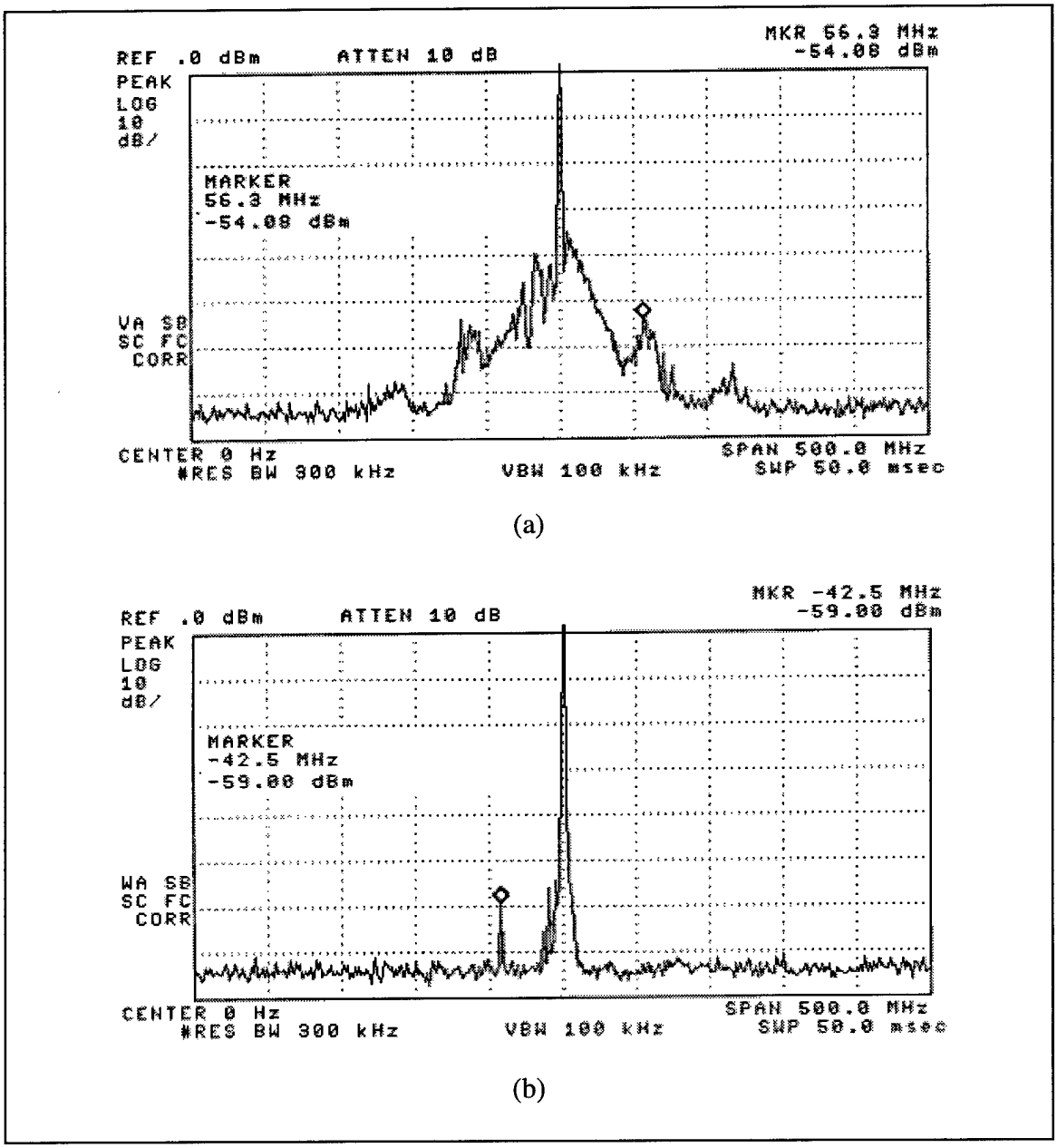

Figure 28. SBS RF spectrum (500 MHz span) for two laser beams coupled into a single-pass setup with 33 mW of input power. (a) SBS RF Spectrum, (b) RF spectrum for no signal.

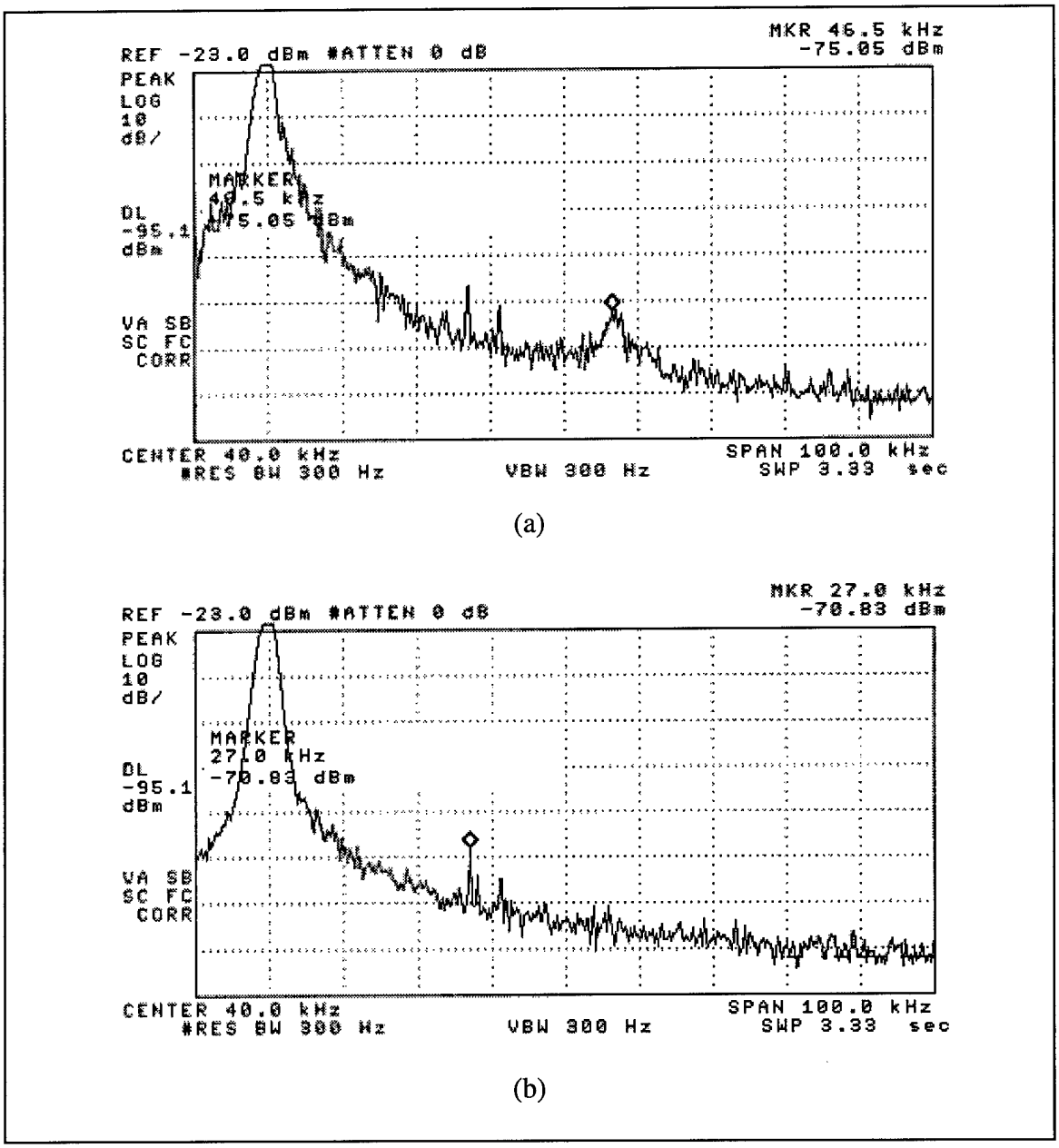

Figure 29. SBS RF spectrum (100 kHz span) for two laser beams coupled into a fiber ring setup with 33 mW of input power. (a) SBS RF spectrum, (b) RF spectrum for no signal.

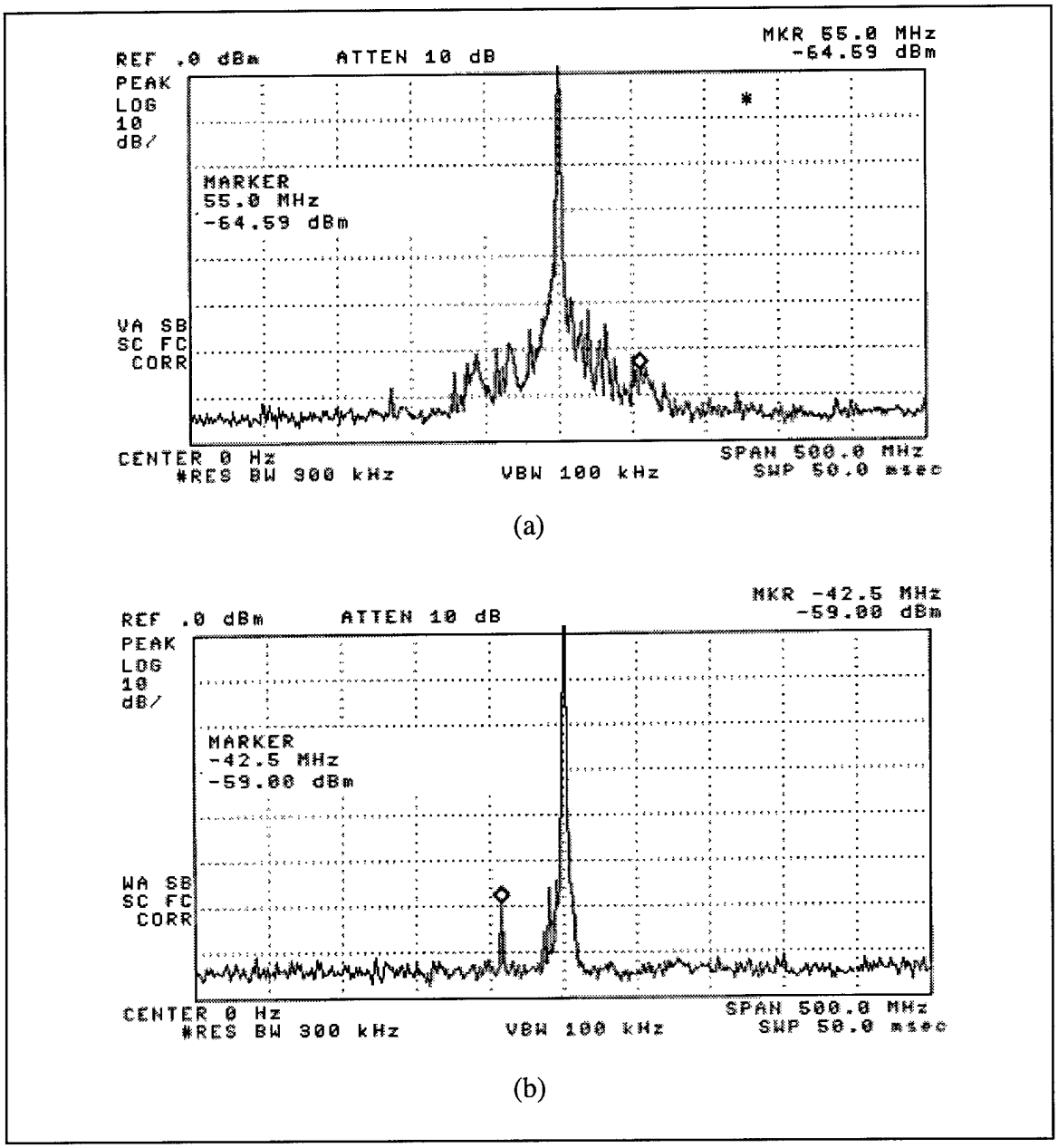

Figure 30. SBS RF spectrum (500 MHz span) for two laser beams coupled into a fiber ring setup with 22.5 mW of input power. (a) SBS RF spectrum, (b) RF spectrum for no signal.

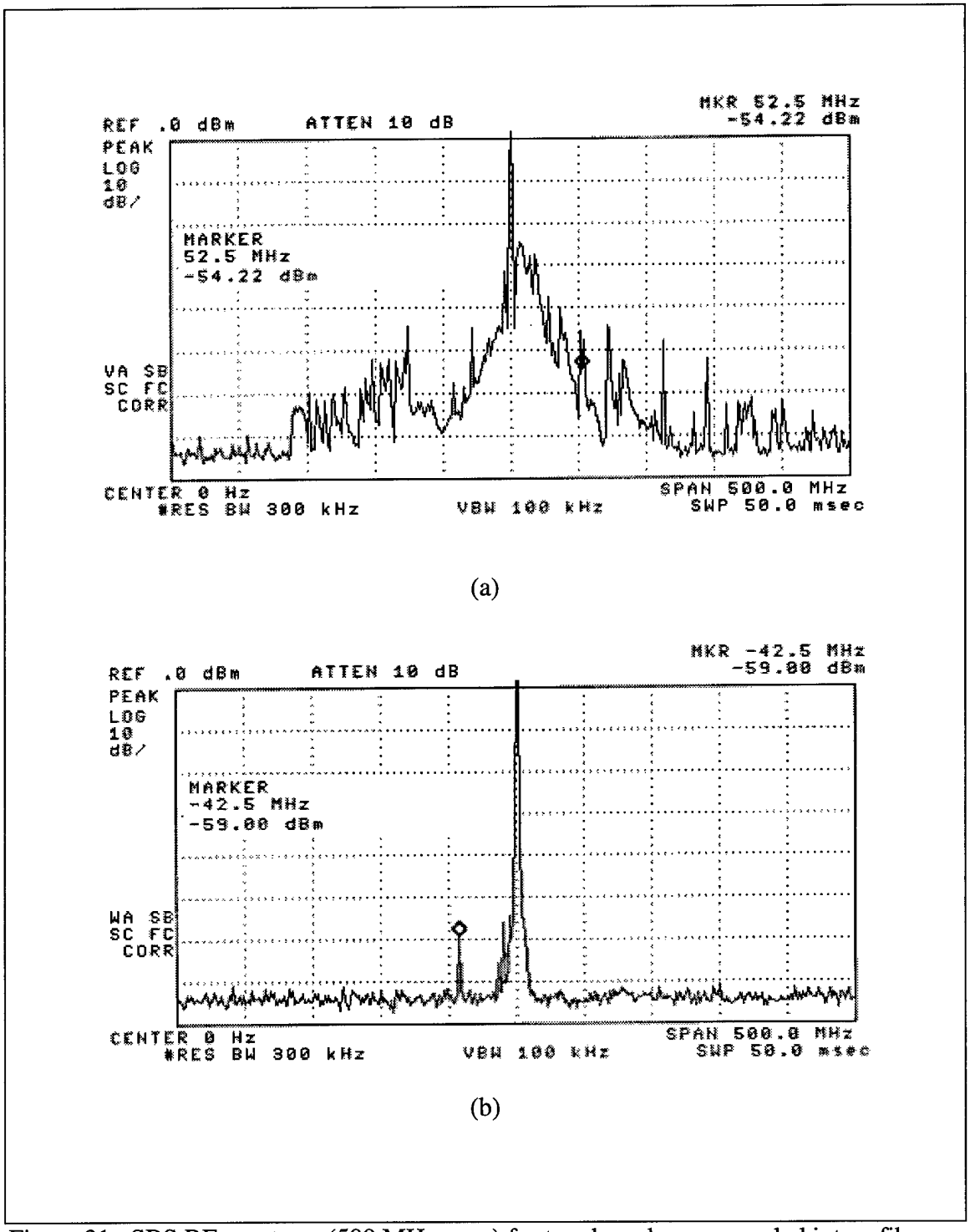

Figure 31. SBS RF spectrum (500 MHz span) for two laser beams coupled into a fiber ring setup with the pump laser at maximum power (45 mW of input power). (a) SBS RF spectrum, (b) RF spectrum for no signal.

31 were a result of the erratic behavior of the SBS signal and changed at random. The behavior most likely can be attributed to the chaotic nature of SBS mentioned previously.

A plot of the SBS power as a function of input power is shown in Figure 32. The threshold power of the single-pass case was found to be 26.4 ± 0.5 mW. The SBS power

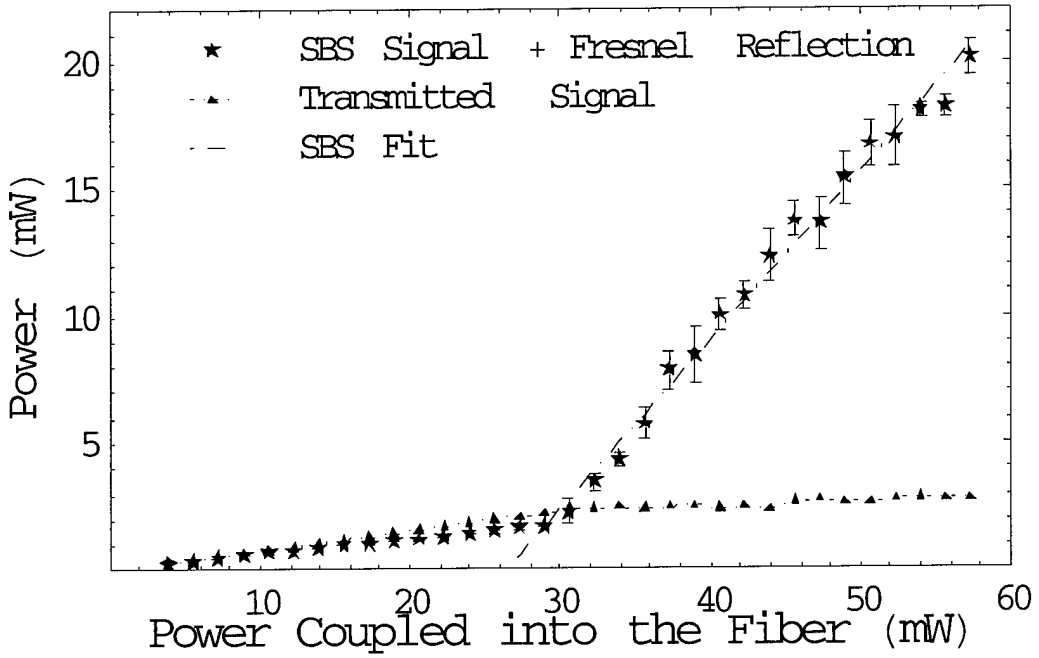

Figure 32. SBS and transmitted power vs. power coupled into the fiber for the two beam, single laser, single-pass setup.

conversion slope efficiency was 36%. Figure 33 shows the SBS power as a function of input power for the two beam, fiber ring setup. A comparison of Figure 33 with Figure 13 shows very little difference in the single beam and two beam SBS threshold power. The threshold power for the fiber ring case was 19.0 ± 0.5 mW. This is within the experimental error of the single laser beam case. The SBS power conversion slope efficiency was 47%. The maximum SBS power achieved was 26.5 mW. The maximum

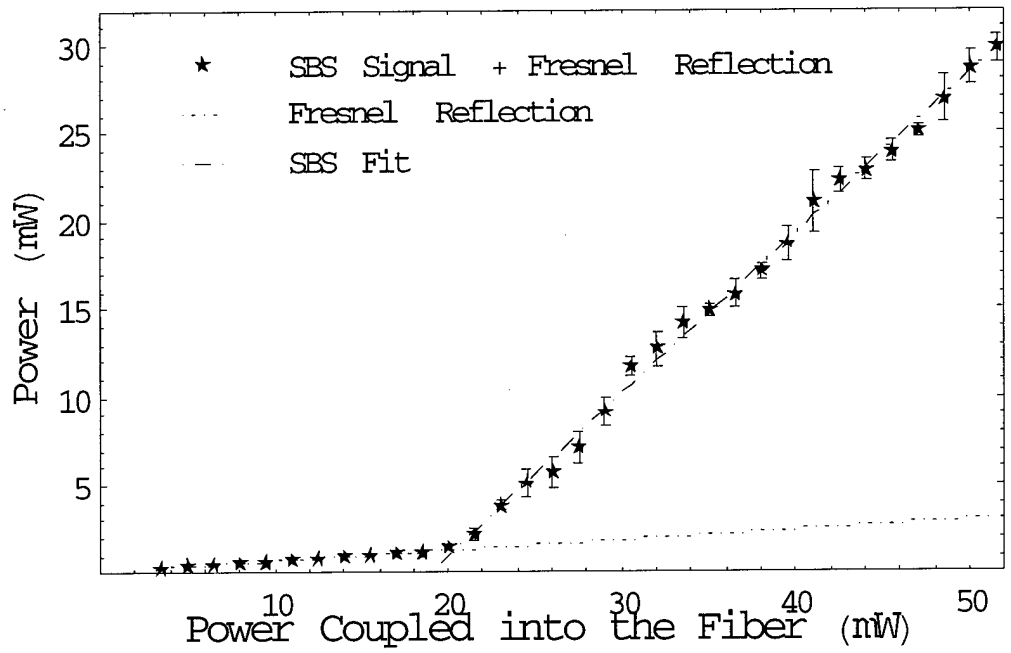

Figure 33. SBS power vs. power coupled into the fiber for the two beam, single laser, fiber ring setup.

SBS power was lower than the single laser beam case because it is more difficult to achieve a high coupling efficiency when more than one beam must be aligned into the fiber. Unless the two beams are traveling the exact same path when entering the fiber, the coupling efficiency will be reduced because one beam will be at a slightly different location or angle from the other beam.

The polarization of the SBS beam was dependent on the ratio of the powers of the two beams. The dominant of the two beams dominated the SBS polarization. For instance, when the power of the horizontally polarized beam dominated the power of the vertically polarized beam, the SBS beam was linearly polarized in a direction close to horizontal.

The SBS intensity real time oscilloscope traces were similar to the single beam case. No visible difference could be seen in the SBS oscillations and amplitude fluctuations when comparing the traces from the one and two beam cases.

The SBS signal was viewed with a frame grabber and BeamCode software to compare it to the input laser beams. The BeamCode contour plots are shown in Figure 34. Figures 34a and 34b show the reflection of each of the two beams entering the fiber. The reflection from the two beams together is shown in Figure 34c. Figure 34d shows the resulting SBS signal created by the two beams. At the power level for Figure 34d, no SBS signal was created unless both beams were coupled into the fiber. The SBS signal at the maximum laser power is shown in Figure 34e. The small shift of the SBS signal to the left shown in Figure 34d and 34e is a result of adjusting the beam splitter in front of the camera to decrease the amount of light reaching the camera to prevent over saturation. The SBS signal location did not move as the angles at which the pump beams were coupled into the fiber were adjusted or as the laser power was increased.
From Figure 34 it is apparent that the SBS signal created from two beams is a good Gaussian shape. Most of the distortion shown in the contour plot in Figure 34 is a result of the Fresnel reflection overlapping the SBS signal. As the input power is increased further above threshold, the SBS signal becomes much greater in power compared to the Fresnel reflection. Depending on the angles in which the two beams are entering the fiber, the Fresnel reflection can also be partially separated from the SBS signal by using an aperture. The images shown in Figure 34 are for the case of two beams exciting SBS in a fiber ring. The results of the single-pass case were similar to that shown in Figure 34 so no images have been shown.

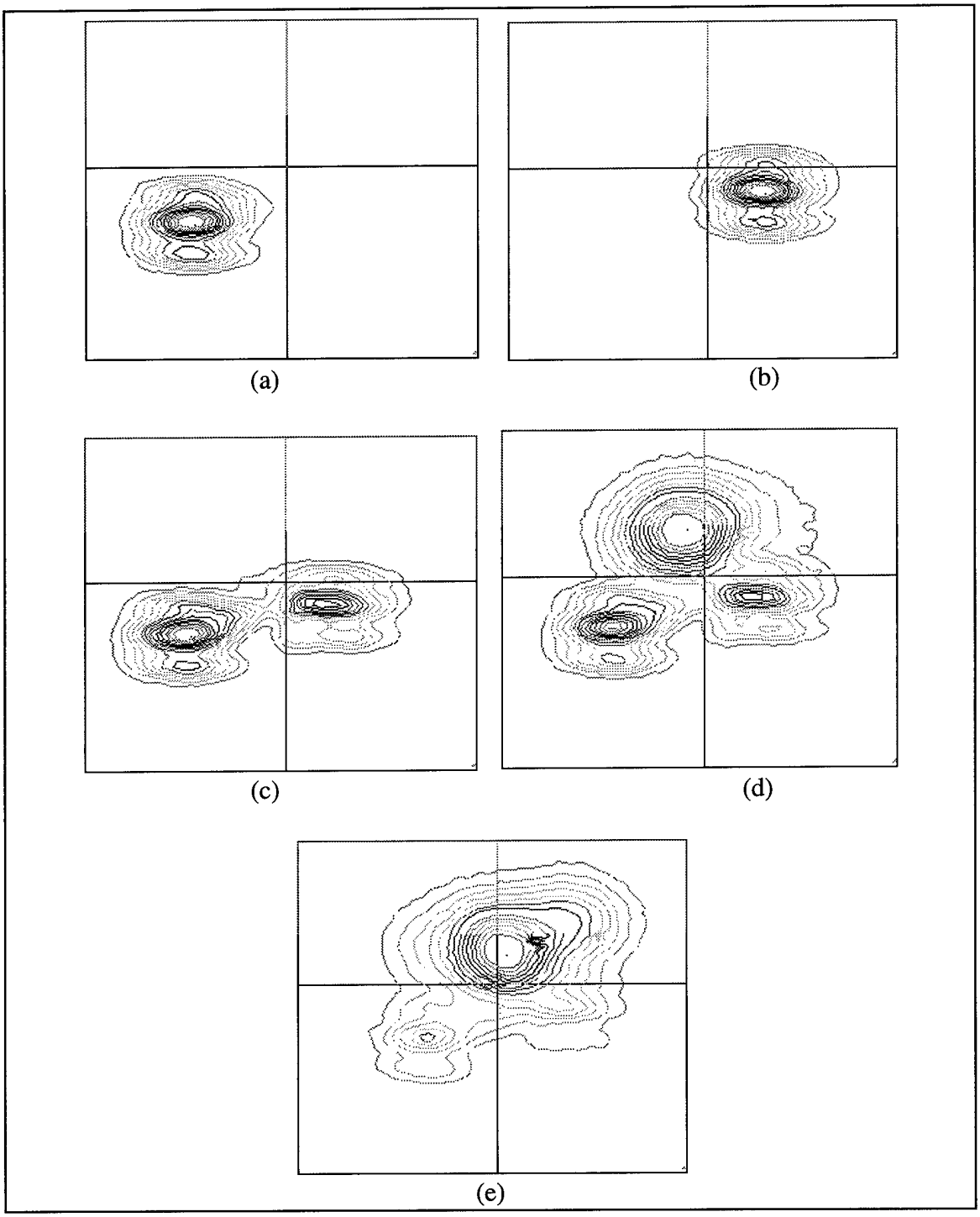

Figure 34. Contour plot of the SBS signal and the Fresnel reflection of the input laser beams for the single laser, two beam, fiber ring setup. (a) Fresnel reflection for leg 1 only, (b) Fresnel reflection for leg 2 only, (c) Fresnel reflection for both legs at a power below the SBS threshold, (d) SBS and Fresnel reflection at the same power as a and b, (e) SBS and Fresnel reflection at maximum pump laser power.

The beam-in-a-bucket experiment was performed for both the fiber ring and the single-pass case. As mentioned in the previous chapter, a perfect Gaussian beam should give a result of 95.5%. For the single-pass case, the experiment resulted in a ratio of 83.5 ± 0.1%. For the fiber ring case, the experiment resulted in a ratio of 83.8 ± 0.1%. While the experiment did not yield the ratio expected for a perfect Gaussian, it is a reasonable value. Any turbulence in the air as well as all of the optics serve to distort a perfect Gaussian so that it is unrealistic to expect to have a perfect Gaussian beam. Therefore, it can be concluded that the beam combining produced a very good quality beam.

The beam cleanup ability of the two beams was also investigated. As with the single beam cleanup, the results were very good. The results of the beam cleanup are shown in Figure 35. It can be seen from Figures 35d that the resulting SBS beam is a good Gaussian shape.

5.4 SBS Fiber Gain Measurement

The fiber SBS gain was measured in a 50 μm diameter multi-mode fiber as discussed in the experimental setup. A 50 μm fiber was used for this measurement in hopes that eventually it could be used for combining laser beams instead of the 9.5 μm diameter fiber. The larger diameter fiber has the advantage that it is much less sensitive to small changes in the alignment of the laser and has a higher coupling efficiency. The resulting gain curve for the 50 μm diameter fiber is shown in Figure 36. The data points have been fit with both a Gaussian and a Lorentzian line shape. Neither curve is a perfect fit, however the data points fit the Lorentzian fairly well. Theoretically the curve should be a Lorentzian, however it is expected that the curve will not be a true Lorentzian since inhomogeneities in the fiber modify the line shape [5].

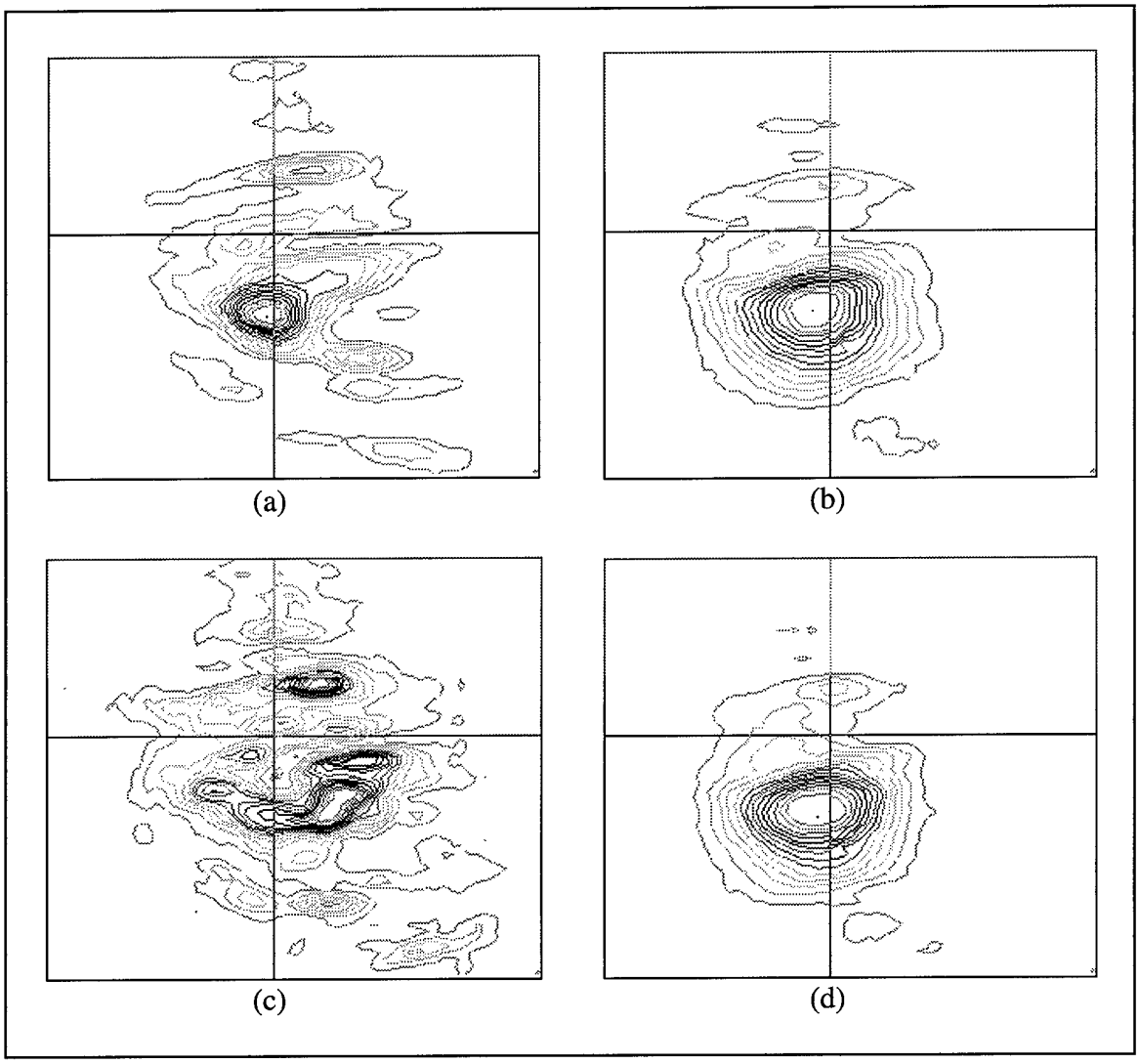

Figure 35. Contour plot of the SBS signal and the Fresnel reflection of the two laser beams for both aberrated and unaberrated beams in the two beam, single laser, fiber ring setup. (a) Unaberrated input laser beams, (b) SBS and input laser beams for Unaberrated case, (c) Aberrated input laser beam, (d) SBS and input laser beams for aberrated case.

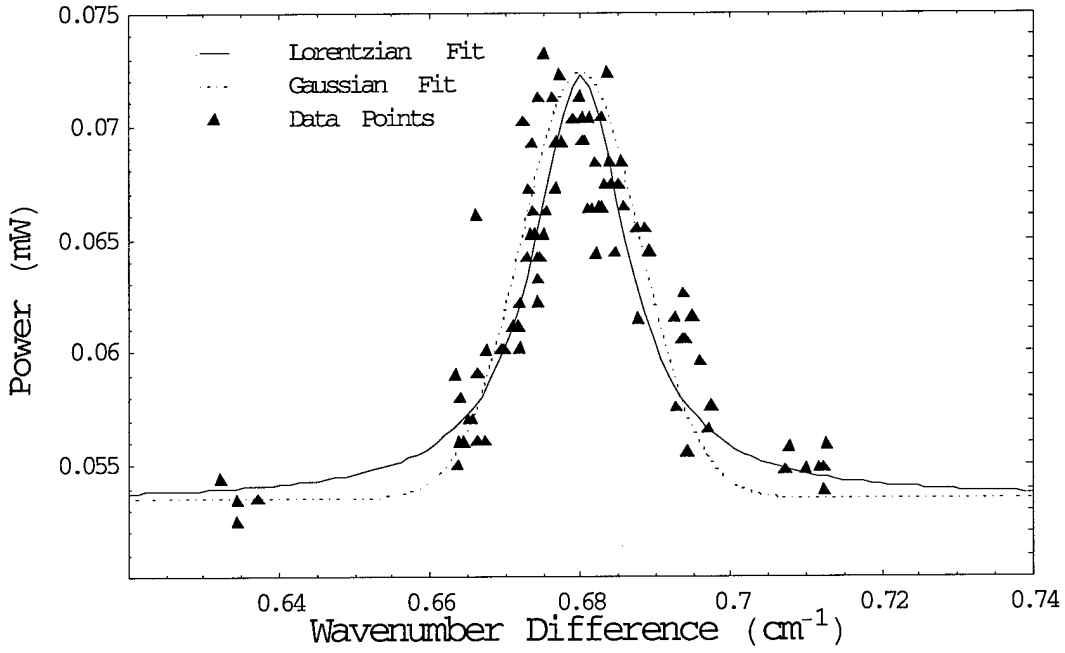

Figure 36. SBS gain spectrum for the 50 μm diameter silica fiber. $1/\lambda_S = 12403.56\ cm^{-1}$, $1/\lambda_P = (12403.56 + \text{Wavenumber Difference})\ cm^{-1}$, $P_P(0) = 58.5$ mW, $P_S(L) = 17.6$ mW, $\alpha = 3.2$ dB/km.

The line width of the gain spectrum in Figure 36 is 500 MHz. The intrinsic line width of the gain spectrum is determined by $\Delta\nu_B = \Delta\nu_B' - 2\,\Delta\nu_L$ where $\Delta\nu_B'$ is the line width determined in Figure 36 and $\Delta\nu_L$ is the laser line width [26]. The laser line width was 140 MHz. This gives an intrinsic line width of 220 MHz for the Brillouin gain spectrum. The line width in bulk silica is approximately 17 MHz for a pump wavelength of 1.525 μm [5]. Since the line width is proportional to $1/\lambda^2$, the line width in bulk silica for a pump wavelength of 807 nm is expected to be approximately 61 MHz. As discussed in Chapter II, the line width in silica fibers is typically much broader because of inhomogeneities in the fiber. Therefore, the intrinsic line width of 220 MHz for the Brillouin gain spectrum is within the expected range of values.

From the gain spectrum shown in Figure 36, the peak SBS gain coefficient can be determined. Using the pump power, Stokes power, fiber loss, and power gain measurements from numerous trials, the average gain coefficient was determined by numerically solving Equations 13 and 14 using a Runge-Kutta method. The gain coefficient was calculated to be 0.79 ± 0.44E-11 m/W. The commonly accepted value for the SBS gain coefficient of silica fibers is 5E-11 m/W [4:269]. From Equation 19 the experimental value of the gain coefficient gives an SBS threshold power of 3.68 W, while the expected gain coefficient gives a threshold power of 0.58 W. Some of the error in the experimental value is caused by the instabilities in the laser wavelength.

For the 50 μm diameter fiber to be used in a practical system to combine diode laser beams, very powerful diode lasers would have to be used. While multi-watt diode lasers exist, most single-mode diode lasers have a maximum power of less than 500 mW. Using SBS for combining the beams, however, requires that the lasers be single-mode lasers. Since SRS does not require that the lasers be single-mode lasers, the SRS gain coefficient was also measured.

5.5 Raman Fiber Gain Measurement

The Raman gain coefficient was measured using the setup shown in Figure 12. The power gain measured by the lock-in amplifier and the input and transmitted DC power of both the pump and Stokes lasers was used to calculate the Raman gain coefficient by numerically solving Equations 25 and 26. The gain coefficient was calculated to be 2.6 ± 0.1E-13 m/W at a pump to Stokes wavenumber difference of 386.87 cm^{-1}. The maximum theoretical Raman gain coefficient for a silica fiber at a pump wavelength of 808 nm is 1.2E-13 m/W [10, 4:220]. From Equation 27 the

experimental value of the gain coefficient gives an SRS threshold power of 221 W for the fiber used. This is a very impractical threshold power. For SRS to be used instead of SBS to combine two or more laser beams practically, the threshold power would have to be much lower. The threshold power could be reduced to below 1 W by using a fiber longer than 20 km with a pump wavelength of approximately 1.5 μm and a fiber diameter on the order of 5 μm. While changing the pump wavelength reduces the fiber loss significantly and can be done for some applications, reducing the diameter of the fiber by a factor of 10 adds other problems. With small fibers it is much harder to align the beams into the fiber. This reduces the coupling efficiency and makes the system much more sensitive to very minor adjustments in the laser beam alignment. A practical system must not be so sensitive to adjustments. Therefore, using SRS for combining diode laser beams would not be practical unless hundreds of multi-watt diode lasers are used.

VI. Conclusions and Recommendations

6.1 Conclusions

In this thesis research, we have confirmed the beam cleanup properties of the SBS process in a long multi-mode fiber, as was first demonstrated by Bruesselbach. The SBS beam had a very nice Gaussian shape. The SBS beam did not change its position as viewed by the frame grabber while the pump laser beam power and input angle were adjusted and the beam aberrated. For the 9.5 μm diameter fiber used, the SBS threshold power was 26.5 ± 0.5 mW for the single-pass setup and 19.7± 0.5 mW for the fiber ring setup. The pump to SBS power conversion slope efficiency was found to be 42% and 52% for the single-pass and the fiber ring setups respectively. The SBS intensity oscillated as a result of pump depletion. It is expected that higher pump powers would result in a steady SBS signal. There were also erratic amplitude fluctuations in the SBS signal. This could be a result of the chaotic nature of SBS reported by Harrison *et al.* [15].

In addition to the beam cleanup demonstrated, we have generalized the concept to include the combining of two beams into a single coherent beam. Using SBS in a multi-mode fiber for this purpose was successful. The SBS threshold power for both the two beam, single-pass setup and the two beam, fiber ring setup were within the experimental error of the single beam setups. There was no visible difference in the SBS oscillations or erratic amplitude fluctuations when compared with the single beam case. The beam-in-a-bucket experiment resulted in a value of 83.5 ± 0.1% and 83.8 ± 0.1% for the single-pass and fiber ring setups respectively. This indicates a very good Gaussian shaped beam. The frame grabber images also indicated a very good Gaussian shaped beam, even

when the input beams were aberrated. When the power of each of the two input beams individually were below the SBS threshold of the fiber, the SBS signal was created only when both beams were coupled into the fiber and the combined power of the two beams was above the SBS threshold power. The SBS beam was polarized the same as that of the dominant input beam. For instance if the horizontally polarized input beam power was much greater than the power of the vertically polarized beam, then the SBS signal was linearly polarized at an angle close to horizontal.

A summary of the fiber gain coefficient measurements is shown in Table 1. The measurements are for the 50 μm diameter fiber. The threshold power for SBS was determined using Equation 19. The threshold power for SRS was determined using Equation 27. The SRS gain coefficient was measured with a pump to Stokes wavenumber difference of 386.87 cm^{-1}. While some modifications could be made to the system to reduce the SRS threshold power, it is not yet a practical system for combining diode laser beams. Ideally a threshold power below one watt would be needed. This requires the SRS gain coefficient to be on the order of the SBS gain coefficient.

Table 1. Summary of the SBS and SRS measurements for the 50 μm diameter fiber.

Process	Gain Coefficient		Threshold Power	
	Measured Value (m/W)	Accepted Value (m/W)	Using Measured Gain Coefficient (W)	Using Accepted Gain Coefficient (W)
SBS	0.79 ± 0.44E-11	5E-11 [4:269]	3.68	0.58
SRS	2.6 ± 0.1E-13	1.2E-13 [10, 4:220]	221	479

While the narrow SBS gain spectrum placed a strict constraint on the wavenumbers of the lasers being combined, the beam combining via SBS in multi-mode

optical fibers was very successful. The 52% pump to SBS power conversion efficiency provides a very efficient method for combining multiple laser beams. The low threshold power for SBS in optical fibers makes it ideal for combining the beams from many diode lasers. Assuming the lasers can be maintained at matched wavelengths, SBS in multi-mode optical fibers is the ideal solution. The beam cleanup capabilities of SBS provide a very good quality beam from even very aberrated pump beams. While maintaining the wavelengths of the lasers is a problem that must be resolved, SBS in multi-mode optical fibers has been shown to be a very efficient and effective method for combining multiple diode laser beams. This result will allow the Air Force to combine the beams of hundreds of thousands of diode lasers into one coherent high power laser beam that could be used for tactical weapon systems as well as many other applications. The high efficiencies of both the diode lasers and the beam combining result in a much lower input power that is needed and a smaller, lighter system.

As mentioned above, the major roadblock to using SBS in multi-mode optical fibers to combine multiple laser beams is the constraint on the laser wavelengths. One possible solution to this is the use of SRS instead of SBS. While the threshold power for SRS is much higher, it does not place such a strict constraint on the wavelengths of the input lasers. Therefore, it is very likely that SRS in multi-mode optical fibers could be used to combine the laser beams.

Both SBS and SRS in multi-mode optical fibers show great promise for combining the laser beams from many diode lasers. The end result of such a system would be ideal for both air borne and space borne weapon systems. Further research must be performed before this can be used in a fielded weapon system. However, the

initial research suggests that either SBS or SRS will be an integral part of any system combining the beams of many diode lasers. It is recommended that the Air Force continue this research. Some recommendations for future research are outlined in the next section of this chapter.

6.2 Recommendations

Further investigation is needed before SBS and SRS can be used in a practical system for combining laser beams. This section will present some recommendations for future research. The majority of the recommendations deal with reducing the SBS and SRS threshold power since this would allow larger diameter fibers to be used.

The first recommendation is to investigate the use of both doped silica fibers as well as halide fibers. Doping silica fibers with various materials such as GeO_2 changes the SBS and SRS gain coefficients. While research by Shibata, *et al.* shows that GeO_2 doping decreased the Brillouin gain, it is possible that a different doping material could be found to increase the Brillouin gain [27]. Since the gain depends on the material properties, other types of fibers should also be investigated. Hwa, *et al.* have shown that halide glass has a higher Brillouin gain coefficient [28]. Cotter has suggested that fibers made of halide glass could have a threshold power as low as tens of microwatts [29].

Another way to decrease the threshold power in a fiber is to seed the fiber with the Stokes wave from the exit end of the fiber. Similar to creating a fiber ring, this would lower the threshold power allowing for the use of the larger diameter fibers.

The use of tapered fibers should also be investigated. A tapered fiber could be used to provide a large diameter at the input end of the fiber while keeping the majority

of the fiber at a much smaller diameter. This would reduce the sensitivity to the pump beam alignment without having a large effect on the SBS and SRS threshold powers.

It was expected that when the quarter wave plate was inserted in the path of the beam and rotated 45 degrees, the polarization of the SBS beam should be the same as the Fresnel reflection. Since the polarization remained the same as the input beam, the polarization of the SBS beam should also be investigated.

A method must also be found to separate the SBS beam from the input beam since the quarter wave plate did not work. Also a more efficient method must be found to couple many more beams into the fiber. The use of a graded index lenses should be investigated to solve both of these problems. The basic experimental setup is shown in Figure 37. The beams would be coupled into patch cords, which are bundled around the output patch cord, as shown in the patch cord cross section in Figure 37. The graded index lenses would collimate the beams. The beams would then be focused and coupled into the fiber that is used to produce the SBS beam. The SBS beam would travel back to the bundle of patch cords and be coupled into the center patch cord. This would serve to separate the SBS beam from the input beams as well as couple at least 6 beams into the fiber. More beams could be added by adding more patch cords to the outside of the bundle of patch cords.

Finally the generation of a single spatial mode SBS beam made up of two frequencies of light should be investigated. This could be done by using two lasers that have frequencies separated by at least 100 MHz. The separation in the two laser frequencies is enough to completely separate the two SBS gain curves for the two pump

frequencies. While the resulting beam would not be good for most applications, it would be a good method for achieving a high power beam on a target.

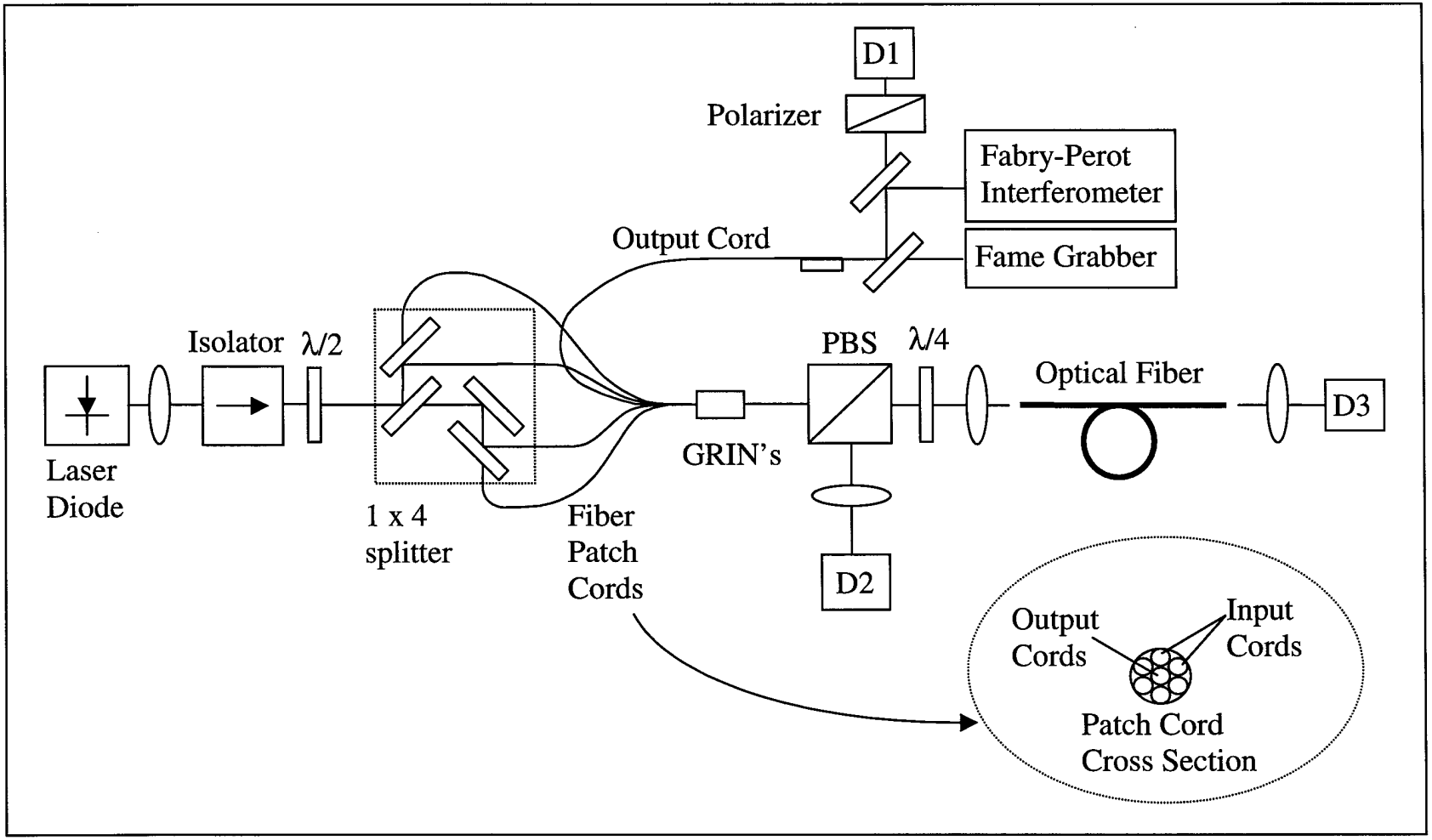

Figure 37: Suggested experimental setup for coupling many beams into one fiber and separating the SBS beam from the input beams.

Bibliography

1. J. A. Tirpak. A massive study considers the Air Force's place in the future that will be much different from today. *Air Force Magazine*, 20-24, December, 1996.

2. J.T. Verdeyen. *Laser Electronics.* Prentice-Hall, Inc., New Jersey, 1995.

3. R.W. Boyd. *Nonlinear Optics.* Academic Press, Inc., New York, 1992.

4. G.P. Agrawal. *Nonlinear Fiber Optics.* Academic Press, Inc., New York, 1989.

5. R.W. Tkach, A.R. Chraplyvy, and R.M. Derosier. Spontaneous Brillouin Scattering for Single-Mode Optical-Fibre Characterization. *Electron. Lett.*, 22:1011-1013, September 1986.

6. E. Lichtman, A.A. Friesem, R.G. Waarts, and H.H. Yaffe. Stimulated Brillouin Scattering Excited by a Multi-mode Laser in Single-Mode Optical Fibers. *Opt. Comm.*, 64:544-548, December 1987.

7. E.P. Ippen and R.H. Stolen. Stimulated Brillouin Scattering in Optical Fibers. *Appl. Phys. Lett.*, 21:539-541, December 1972.

8. C.L. Tang. Saturation and Spectral Characteristics of the Stokes Emission in the Stimulated Brillouin Process. *J. Appl. Opt.*, 37:2945-2955, July 1966.

9. I. Bar-Joseph, A.A. Friesem, E. Lichtman, and R.G. Waarts. Steady and Relaxation Oscillations of Stimulated Brillouin Scattering in Single-Mode Optical Fibers. *J. Opt. Soc. Am. B*, 2:1606-1611, October 1985.

10. R.H. Stolen. *Proc. IEEE*, 68:1232, 1980.

11. R.Y. Chiao, C.H. Townes, and B.P. Stoicheff. Stimulated Brillouin Scattering and Coherent Generation of Intense Hypersonic Waves. *Phys. Rev Lett.*, 12:592, 1964.

12. D. Cotter. Observation of Stimulated Brillouin Scattering in Low Loss Silica Fiber at 1.3 Micron. *Electron. Lett.*, 18:495-496, June 1982.

13. N. Uesugi, M. Ikeda, and Y. Sasaki. Maximum Single Frequency Input Power in a Long Optical Fiber Determined by Stimulated Brillouin Scattering. *Electron. Lett.*, 17:379-380, May 1981.

14. A. Gaeta and R.W. Boyd. Stochastic Dynamics of Stimulated Brillouin Scattering in an Optical Fiber. *Phys. Rev. A*, 44:3205-3209, September 1991.

15. R.G. Harrison, J.S. Uppal, A. Johnstone, and J.V. Moloney. Evidence of Chaotic Stimulated Brillouin Scattering in Optical Fibers. *Phys. Rev. Lett.,* 65:167-170, July 1990.

16. K.O. Hill, B.S. Kawasaki, and D.C. Johnson. CW Brillouin Laser. *Appl. Phys. Lett.*, 28:608-609, May 1976.

17. D.R. Ponikvar and S. Ezekiel. Stabilized Single-Frequency Stimulated Brillouin Fiber Ring Laser. *Opt. Lett.*, 6:398-400, August 1981.

18. L.F. Stokes, M. Chodorow, and H.J. Shaw. All-Fiber Stimulated Brillouin Ring Laser with Submilliwatt Pump Threshold. *Opt. Lett.*, 7:509-511, October 1982.

19. M. Gower, and D. Proch. *Optical Phase Conjugation.* Springer-Verlag, New York, 1994.

20. N.G. Basov, V.F. Efimkov, A.V. Kotov, A.B. Mironov, S.I. Mikhailov, and M.G. Smirnov. *Sov. J. Quantum Electron.*, 9:455, 1979.

21. M. Valley, G. Lombardi, and R. Aprahamian. Beam Combination by Stimulated Brillouin Scattering. *J. Opt. Soc. Am. B*, 3:1492-1497, October 1986.

22. T.R. Loree, D.E. Watkins, T.M. Johnson, N.A. Kurnit, and R.A. Fisher. Phase Locking Two Beams by Means of Seeded Brillouin Scattering. *Opt. Lett.*, 12:178-180, March 1987.

23. S. Sternklar, D. Chomsky, S. Jackel, and A. Zigler. Misalignment Sensitivity of Beam Combining by Stimulated Brillouin Scattering. *Opt. Lett.*, 15:469-470, May 1990.

24. E.A. Kuzin, M.P. Petrov, and B.E. Davydenko. Phase Conjugation in an Optical Fibre. *Opt. and Quant. Elect.*, 17:393-397, 1985.

25. H. Bruesselbach. Beam Cleanup Using Stimulated Brillouin Scattering in Multi-Mode Fibers. *Conference on Lasers and Electro-Optics.* CLEO 1993, 424-425, 1993.

26. Y. Azuma, N. Shibata, T. Horiguchi, and M. Tateda. Wavelength Dependence of Brillouin-Gain Spectra for Single-Mode Optical Fibres. *Elect. Lett.*, 24:250-252, March 1988.

27. N. Shibata, R.G. Waarts, and R.P. Braun. Brillouin-gain spectra for single-mode fibers having pure-silica, GeO_2-doped, and P_2O_5-doped cores. *Opt. Lett.*, 12:269-271, April 1987.

28. L. Hwa, J. Schroeder, and X. Zhao. Intrinsic Brillouin linewidths and stimulated Brillouin gain coefficients in glasses studied by inelastic light scattering. *J. Opt. Soc. Am. B,* 6:833-839, April 1987.

29. D. Cotter. *J. Opt. Commun.,* 4:10,1983.

Vita

First Lieutenant Blake C. Rodgers was born on July 25, 1973, in Abington, Pennsylvania. He graduated from Pennridge High School in 1991 and then attended the United States Air Force Academy. He graduated in 1995 with a degree of Bachelor of Science in Physics. Upon graduation, he received a commission in the United States Air Force and was assigned to the National Air Intelligence Center. He worked as a computer aided design application programmer until entering the School of Engineering, Air Force Institute of Technology, in August, 1997.

Permanent address: 408 Creek Rd.
Pippersville, PA 18947

REPORT DOCUMENTATION PAGE

Form Approved
OMB No. 0704-0188

1. AGENCY USE ONLY *(Leave blank)*	2. REPORT DATE	3. REPORT TYPE AND DATES COVERED
	March 1999	Master's Thesis

4. TITLE AND SUBTITLE
Laser Beam Combining and Cleanup via Stimulated Brillouin Scattering in Multi-mode Optical Fibers

5. FUNDING NUMBERS

6. AUTHOR(S)
Blake C. Rodgers, First Lieutenant, USAF

7. PERFORMING ORGANIZATION NAME(S) AND ADDRESS(ES)
Air Force Institute of Technology
2750 P Street
Wright-Patterson AFB, OH 45433-7765

8. PERFORMING ORGANIZATION REPORT NUMBER
AFIT/GAP/ENP/99M-09

9. SPONSORING/MONITORING AGENCY NAME(S) AND ADDRESS(ES)
Air Force Research Lab (AFRL/DELS)
3550 Aberdeen Ave SE
Kirtland AFB, NM 87117-5776

10. SPONSORING/MONITORING AGENCY REPORT NUMBER

11. SUPPLEMENTARY NOTES

12a. DISTRIBUTION AVAILABILITY STATEMENT
Approved for public release; distribution unlimited

12b. DISTRIBUTION CODE

13. ABSTRACT *(Maximum 200 words)*

The main objective of this thesis was to demonstrate the feasibility of combining and cleaning up multiple laser beams via Stimulated Brillouin Scattering (SBS) in a multi-mode optical fiber. Beam combining via SBS in an optical fiber is of interest because of the low SBS threshold power in an optical fiber allowing low power diode laser beams to be combined into one high power beam. SBS theory and some of the important historical results are described briefly.

The experimental results clearly indicate that SBS in multi-mode optical fiber can indeed combine laser beams and clean up the beams at the same time. Both single-pass and ring-cavity geometries were used successfully. The SBS threshold power for the 9.5 micron diameter fiber was 26.5 ± 0.5 mW for a single-pass setup and 19.7 ± 0.5 mW for a ring-cavity setup. The SBS power conversion slope efficiency was measured to be 42% for the single-pass setup and 52% for the ring-cavity setup. The SBS signal exhibited both periodic oscillations and random amplitude fluctuations, which are believed to be due to low levels of power used for the experiment. The polarization of the SBS signal was the same as the input laser beam.

14. SUBJECT TERMS
Laser, Stimulated Brillouin Scattering, SBS, Laser Beam Combining, Laser Beam Cleanup, Stimulated Raman Scattering, SRS, Fiber Optic

15. NUMBER OF PAGES
90

16. PRICE CODE

17. SECURITY CLASSIFICATION OF REPORT	18. SECURITY CLASSIFICATION OF THIS PAGE	19. SECURITY CLASSIFICATION OF ABSTRACT	20. LIMITATION OF ABSTRACT
Unclassified	Unclassified	Unclassified	UL